Archaeol Anthropol Sci (2018) 10:279–304
DOI 10.1007/s12520-016-0354-8

ORIGINAL PAPER

A multi-proxy study of anthropogenic sedimentation and human occupation of Gledswood Shelter 1: exploring an interior sandstone rockshelter in Northern Australia

Kelsey M. Lowe[1,2] · **Susan M. Mentzer**[3,4] · **Lynley A. Wallis**[1,5,6,7] · **James Shulmeister**[1]

Received: 19 July 2015 / Accepted: 14 June 2016 / Published online: 21 June 2016

Abstract Rockshelters contain some of the most important archives of human activity in Australia but most research has focused on artifacts and cultural context. This study explores geomorphological and geoarchaeological approaches for understanding a sandstone rockshelter in interior northern Australia: Gledswood Shelter 1. At this site, magnetic susceptibility and micromorphology techniques were integrated with bulk sedimentology, soil chemistry and geochronology to better understand the record of human impact and site formation processes. The micromorphology studies indicate that primary depositional fabrics, such as graded bedding or laminations, are absent, and sediment structural development is low throughout the entire sequence, with most samples exhibiting a high degree of post-depositional mixing. The sediment magnetic susceptibility analysis reveals magnetic changes coinciding with human occupation, a result of anthropogenic burning. Specifically we highlight that combustion features are prevalent in this sandstone shelter and provide critical insights into the human usage of the shelter.

Keywords Magnetic susceptibility · Micromorphology · FTIR · Combustion features · Rockshelters · Site formation processes · Last glacial maximum

✉ Kelsey M. Lowe
k.lowe4@uq.edu.au

[1] Present address: School of Geography, Planning and Environmental Management, The University of Queensland, Chamberlain Building, St Lucia, Brisbane, QLD 4072, Australia

[2] School of Social Science, The University of Queensland, Michie Building, St Lucia, Brisbane, QLD 4072, Australia

[3] Institute for Archaeological Sciences, University of Tübingen, Rümelinstr. 23, 72070 Tübingen, Germany

[4] School of Anthropology, The University of Arizona, 1009 E. South Campus Dr., Tucson, AZ 85721, USA

[5] Department of Archaeology, Flinders University, GPO Box 2100, Adelaide, SA 5001, Australia

[6] Wallis Heritage Consulting, 1/B Swan Street, Brighton, SA 5048, Australia

[7] Nulungu Research Institute, The University of Notre Dame Australia, PO Box 2287, 88 Guy St, Broome, WA 6725, Australia

Introduction and aims

Issues with rockshelter studies in Northern Australia

Geomorphic and geoarchaeological applications in rockshelter environments have become important techniques for understanding site formation processes and depositional inputs. Until recently, however, most studies globally involving these techniques have focused on calcareous rock shelters (e.g. Farrand 1975; Bailey and Woodward 1997), with only a few completed on sandstone shelters (Abbott 1997). In Australia where old cratonic sandstone shelters are often the most dominant archaeological site type investigated, such applications are even rarer.

Propositions about how and when people colonized the continent are typically based, with only a few exceptions (e.g. Bowler and Price 1998; Veth et al. 2009), on sedimentary and environmental archives preserved in rockshelter sites. Issues of stratigraphy, particularly recognising and dating discrete episodes of human occupation, are key to the effective utilisation of such archives (Farrand 2001; Stein and Farrand 2001; Woodward and Goldberg 2001). However, there are significant gaps in the records as these environments are complex and fragmentary (Bailey and Woodward 1997; Farrand 2001; Woodward and Bailey 2000), and isolating individual occupation surfaces is difficult because of the reoccurrence of

habitation (Bailey 2007; Straus 1990, p. 266). Methodological challenges in sediment analyses as well as the lack of preserved archaeological material — particularly in low density sites — have also hindered interpretation of stratigraphic sequences (O'Connor et al. 1999; Straus 1990; Ward and Larcombe 2003). Finally, ongoing use of a site may result in vertical displacement of artifacts, a consequence of human trampling or bioturbation (cf. David et al. 2007; Gifford-Gonzalez et al. 1985; Hughes and Lampert 1977; Nielsen 1991; Richardson 1992, 1996).

Studies that have used multi-proxy approaches focused on defining the stratigraphic associations between the deepest cultural material and the surrounding sediments (e.g. Bird et al. 2002; David et al. 1997; David et al. 2007). Others have drawn attention to the importance of high-resolution data for regional palaeoecology (Smith 2009), how different geomorphic records can produce different occupation records for determining temporal distributions (Ward 2004), and that increases in the frequency of site use do not reveal changes in site function (Marwick 2005). While these studies demonstrate the importance of analytical techniques, there still appears to be lack of understanding their potential benefits. This is especially true for sites that are important to initial colonization (e.g. Allen and O'Connell 2014; O'Connell and Allen 2004; Williams et al. 2015), biogeographic models of colonization (e.g. Bowdler 1977; Fifield et al. 2001; Hiscock 2008, p. 45; Smith 1989, 1993; Veth 1989) and sites occupied through the last glacial maximum (LGM) (e.g. Hiscock 1988; Lamb 1996; Marwick 2002; Morse et al. 2014; Smith 1989, 2009).

Typically, most Australian sandstone rockshelters formed under tropical and semi-arid conditions, and are part of preserved sandstones hills and escarpments which are the remnants of old river deposits (e.g. David et al. 2007; Clarkson et al. 2015). Collapsed roof/overhangs are common. The shelters sedimentary stratigraphy are generally characterised by containing loose, charcoal-enriched surfaces mixed with fine to medium grained sands that often overly slightly more compact medium to coarse grained sands (Ward 2004). These layers rest on weathered rubble or a bedrock base. Cobbles from previous roof fall events are generally present through the stratigraphic sequence of most shelters. Cultural materials include flaked and stone artifacts, charcoal, ochre, grinding stones and in some sites particularly where shell middens are present in the deposit, processed seeds, bone and shell.

Presently, the literature on site formation processes of sandstone shelters is limited. Gledswood Shelter 1 (GS1) is a site located in the interior of semi-arid tropical northern Australia that can be used as a case study to understand human occupation in a sandstone environment (Wallis et al. 2009). What makes GS1 particularly unique is that it fits the biogeographic models of colonization and could be a site potentially occupied through the last glacial maximum. In this paper, we examine the record of occupation and site formation processes that took place in GS1 using geoarchaeological analysis with particular emphasis on micromorphology and magnetic susceptibility. We address two themes: (1) how low-intensity occupation may be expressed, particularly when primary combustion features such as in situ hearths are absent and (2) why applying a mix of proxies is ideal for old cratonic sandstone environments.

Integrated approaches to the study of sedimentation in rockshelter sites

Micromorphology is a valuable tool for understanding archaeological site formation processes and complex stratigraphy in cave and rockshelter sites (Goldberg and Macphail 2006; Goldberg and Sherwood 2006; Vannieuwenhuyse et al. 2016). The technique may be coupled with analyses of loose sediments, such as grain size, mineral magnetics and soil chemistry, to reconstruct down profile trends within an archaeological sequence. Furthermore, micromorphology is an ideal technique for the identification of geogenic, biogenic and anthropogenic inputs to a site, as well as post-depositional processes that impact the preservation of features and archaeological materials. In situ geochemical analyses, such as Fourier transform infrared microspectroscopy (μ-FTIR) and microscopic x-ray fluorescence (μ-XRF) may be conducted directly on primary and secondary components of archaeological sediments in micromorphological samples using the microcontextual approach (Goldberg and Berna 2010; Mentzer and Quade 2013).

Sediment magnetic susceptibility has also been widely adopted as a means to explore issues about depositional mechanisms and human occupation of rockshelter and cave sites (Ellwood et al. 1997; Ellwood et al. 2004; Herries 2006; Herries and Fisher 2010), yet few such studies have been completed on Australian sites (exceptions include Davidson et al. 1993; Keys 2009; Marwick 2005; Rosendahl et al. 2014). Magnetic susceptibility is a measure of the ease with which a material can be magnetized in the presence of a magnetic field (Thompson and Oldfield 1986, p. 25), and can be used to detect magnetic minerals present in sediments (Evans and Heller 2003). Iron-rich materials are the primary cause for magnetic enhancement and their presence can be due to both cultural or natural processes (i.e. fires, pedogenesis or chemical weathering) (Dalan and Banerjee 1998; Fassbinder et al. 1990; Le Borgne 1960; Linford et al. 2005; Maher and Taylor 1988).

The two techniques are complementary and several researchers (e.g. Allen and Macphail 1987; Woodward et al. 2001) have advocated their combined use in archaeological sites of varied age to study ancient agriculture, weathering processes and human use of fire (e.g. Ajas et al. 2013; Dockrill and Simpson 1994; Marmet et al. 1999; Stahlschmidt et al. 2015; Tsatskin and Nadel 2003; Tsatskin and Zaidner 2014). Magnetic susceptibility provides

information about minerals that are difficult to identify using basic optical properties in thin section. Likewise, micromorphology provides information about the post-depositional history of sediments targeted for magnetic analyses.

In particular, it is important to understand whether magnetic minerals have been mobilized within a sequence following their deposition. Microscopic fabrics and structures indicative of mixing due to bioturbation, human and animal trampling or pedoturbation can be observed in thin section (Banerjea et al. 2013; Kooistra and Pulleman 2010; Kovda and Mermut 2010; Miller et al. 2009). Gravitational settling, seasonal down profile seepage and redistribution of water can cause downward movement of fine sedimentary particles, which can also be observed using micromorphology. Furthermore, chemical diagenesis can impact the interpretation of magnetic signals in archaeological sediments. Pedogenic processes can induce the neoformation of strongly magnetic phases such as magnetite and maghemite (Maher 1998) and, for this reason, soil micromorphology and magnetic susceptibility measurements are integrated in paleoclimatic studies (e.g. Derbyshire et al. 1995). Additional chemical processes that impact magnetic mineral phases include redox reactions induced by groundwater fluctuations and biomineralization (Bazylinski and Moskowitz 1997; Ghiorse and Ehrlich 1992), which may be identified in thin section as iron impregnation and depletion features (Lindbo et al. 2010).

Archaeologically, the integration of the two methods have proven most powerful for the identification of heated sediments and combustion features (Herries and Fisher 2010; Stahlschmidt et al. 2015). Micromorphology is frequently employed in the study of traces of fire in archaeological sites, because the technique facilitates the identification of micro- and macroscopic burned materials and intact or reworked combustion features and human activity (Mentzer 2014; Roebroeks and Villa 2011). In this study, we further explore the potential of coupling magnetic susceptibility measurements with microcontextual analyses on micromorphological samples. To date, no such integrated study has been conducted in Australia.

Environmental and geomorphic setting

Local geology and soils

The GS1 site is located in semi-arid tropical inland northeast Sahul, on the west of the Great Dividing Range in northwest Queensland (Wallis et al. 2009) (Fig. 1a). The local bedrock is the Jurassic-age fluvial and shallow water marine coarse Hampstead Sandstone of the Blythesdale Group that formed part of a thick sequence of sediment infilling the paleo-Carpentaria Basin (Smart 1973, p. 12; Fig. 1b). Regional uplift began in the Late Cretaceous, with higher rates in the east. In combination with downwarping of the Carpentaria Basin, the uplift resulted in the establishment of north-south trending faults expressed on the modern land surface as a series of plateaus bounded on their western flanks by escarpments. The south-facing GS1 overhang occurs in the westernmost of these escarpments, 480 m above sea level (asl). The site is located at a topographic boundary, with the foothills of the Gregory Ranges (600–900 m asl) to the east, and the Strathpark Plains (300–400 m asl) sloping gently to the west and south. Meandering its way across the Strathpark Plains, the Norman River is located 1.5 km to the south, while the Woolgar River is located 25 km to the southeast. The headwaters for both rivers are in the Gregory Ranges, and both ultimately drain westward into the Gulf of Carpentaria (Fig. 1a).

Around GS1, the soil temperature regime is hyperthermic, with an average maximum summer air temperature of 34.5 °C and an average maximum winter temperature of 26 °C (Bureau of Meteorology 2013). The area has a semi-arid soil moisture regime, with annual rainfall averaging 480 mm (Bureau of Meteorology 2013). The thin, weakly developed local soils are classified as Tenosols under the Australian Soil Classification system, characterised by A-horizons atop either unweathered parent material or weak B-horizons containing less than 15 % illuvial clay. In the immediate vicinity of the site, the soil parent material is the sandstone bedrock which is overlain by a quartz sand sheet that abuts the shelter wall. Active soil modification processes in and around GS1 include surface hollowing by macropods, cattle and pigs, and termite activity. The surrounding vegetation primarily comprises Georgetown box (*Eucalyptus microneura*) woodland, with lancewood (*Acacia shirleyi*) and ironwood (*Erythophleum chlorostachys*). Other common species include quinine bush (*Petalostigma banksii*), *Bauhinia cunninghamii*, *Dolichandrone heterophylla*, *Carissa lanceolata*, *Terminalia* spp. and *Melaleuca* spp. The grass layer is dominated by a mixture of three-awn (*Aristida* spp.), ribbon (*Chrysopogon fallax*), blue (*Dicanthium* spp. and *Bothriochloa* spp.), kangaroo (*Themeda australis*) and spear grasses (*Heteropogon contortus*), with rocky areas dominated by spinifex (*Triodia* spp.).

The study site

GS1 is a small overhang formed as a result of cavernous weathering (tafoni) at the base of a weathered 8-m-high Mesozoic sandstone outcrop. It is surrounded by several sandstone outliers and exposed bedrock outcrops (Fig. 2). The shelter is located on the outcrop's southern face. The interior space is about 7 m wide, with a height to the roof of 3–5 m at the drip-line, providing a protected living area. The shelter's walls contain stencilled art and pecked geometric motifs, and the shelter floor is sandy, supporting minimal vegetation. Beyond the drip-line, the lightly wooded ground surface

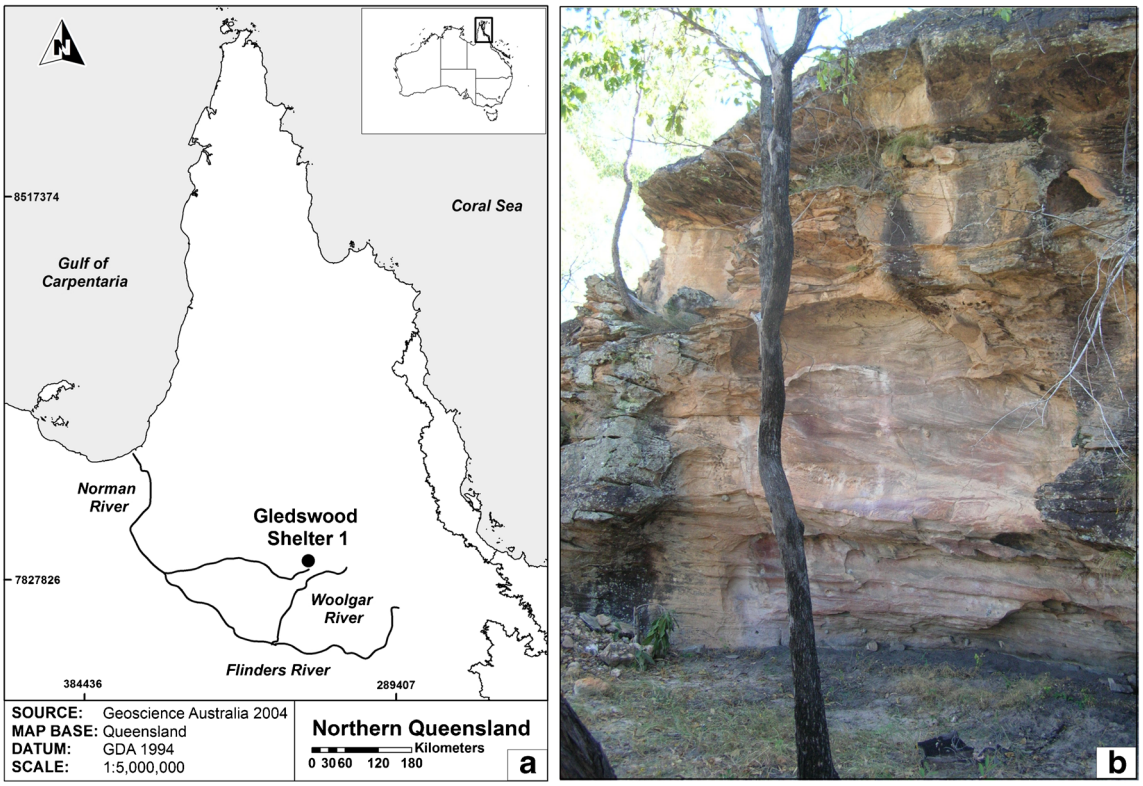

Fig. 1 Map showing the location of Gledswood Shelter 1 in northern Australia (**a**) and view of shelter taken in front of site (**b**). Note from the very top of the shelter to the floor is ~5 m

extends 60 m south and west from the outcrop before dropping down about 15 m on to the Strathpark Plains.

Between the shelter wall and drip-line, six adjoining 1 × 1-m test pits (Squares B0, B1, C0, C1, D0 and D1) were excavated in ~5-cm layers (or spits) to a maximum depth of ca 2.6 m. Square C1 is the main square discussed in this paper. Stratigraphic units (SU) were defined on the basis of field observations of textural and sediment morphological characteristics (Figs. 3 and 4; Table 1). Two depositional areas were also defined. First, the deposits in the more southerly excavation squares are dominated by large quantities of sandstone gravel and cobbles that appear to have fallen from the top of the outcrop just forward of the drip-line. Second, lateral facies changes associated with the morphology of the back wall and living space have resulted in division of the middle sequence into units proximal (SU6a) and distal (SU6b) to the

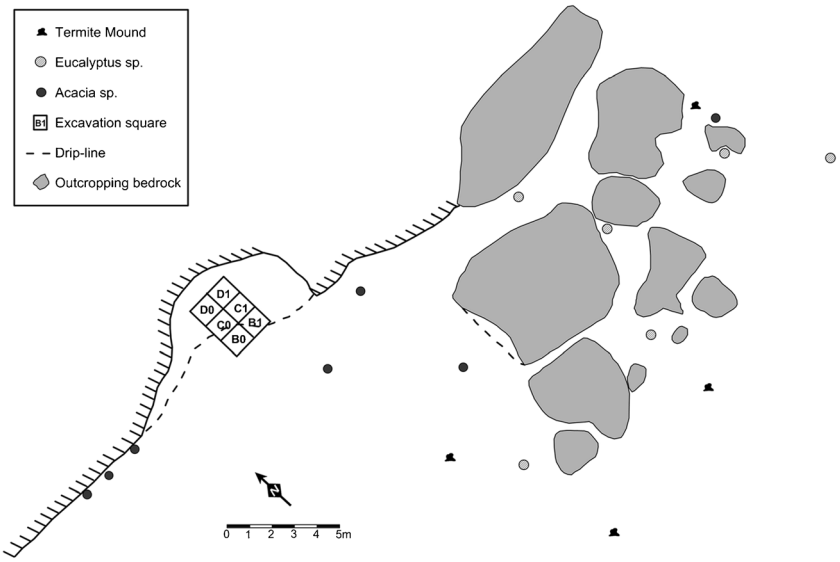

Fig. 2 Site plan map of GS1, showing excavations, shelter dimension and drip-line (Wallis et al. 2009, Fig. 1)

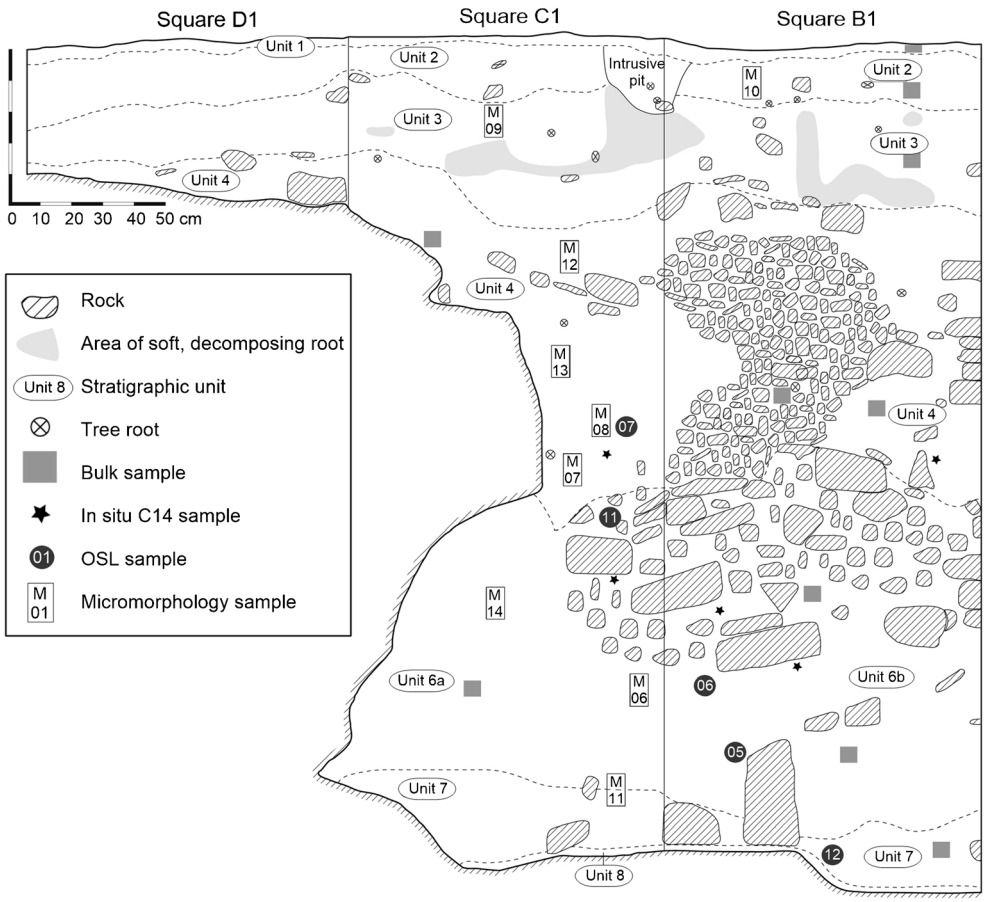

Fig. 3 Cross-section of the shelter and stratigraphy showing Squares D1, C1 and B1

rear wall. Directly below the drip-line, a series of roof fall events have taken place resulting in a large concentration of rock material in Square B1.

SUs 8 and 7 are culturally sterile, with stone artifacts first appearing in low quantities in the middle of SU6, and increasing substantially in abundance at the top of this unit. Stone artifacts are present through SUs 4–1 in varying quantities, as are fragments of ochre and charcoal (Carah 2010; Wallis et al. 2014). Other remains, such as bone and organics, are minimal owing to the acidic conditions. SU5 had been initially defined in the field but was later combined with SU4. Four 50 × 50-cm area control test pits outside the shelter (i.e. 'off-site') were excavated up to 1.2 m depth for the purposes of providing 'natural' samples to compare to the archaeological overhang sediments and to understand the local environment. These sediments consisted of dark greyish brown (10YR 4/2) near the surface to light yellowish brown (10YR 6/4) near the bottom, fine- to medium-sized poorly sorted sands (Table 2 and see Fig. 4).

Initial radiocarbon measurements at the site dated the archaeological deposits to about 28,000 years ago (Wallis et al. 2009). Ages were calibrated using OxCal v.4.2 (Bronk Ramsey et al. 2010) and SHCal13 (Hogg et al. 2013) with ages reported at the 95.4 % confidence level (2σ) (Table 3).

Materials and methods

Detailed sedimentary analysis included stratigraphic description, particle size analysis, loss on ignition (LOI), biologically available phosphorous (P) (the soluble and labile inorganic P component), phytolith analysis, wood charcoal, FTIR and μ-FTIR on loose sediments, micromorphology and analyses of magnetic mineralogies. Bivariate plots were used to help distinguish cultural from natural inputs to the archaeological deposit and to highlight relationships that allowed a better understanding of the site formation processes.

Micromorphology and μ-FTIR

Twelve oriented blocks of sediment were collected for micromorphological analysis (see Fig. 3) and processed at The Australia National University. Samples were first impregnated with polyester resin, and were then sliced into 5 × 7-cm petrographic thin-sections with a standard thickness of 30 μm. The thin sections were analysed at the University of Tübingen using petrographic and stereomicroscopes equipped with plane-polarized, cross-polarized, reflected and oblique incident light (OIL), as well as darkfield illumination and blue light fluorescence. Descriptive criteria followed Stoops (2003).

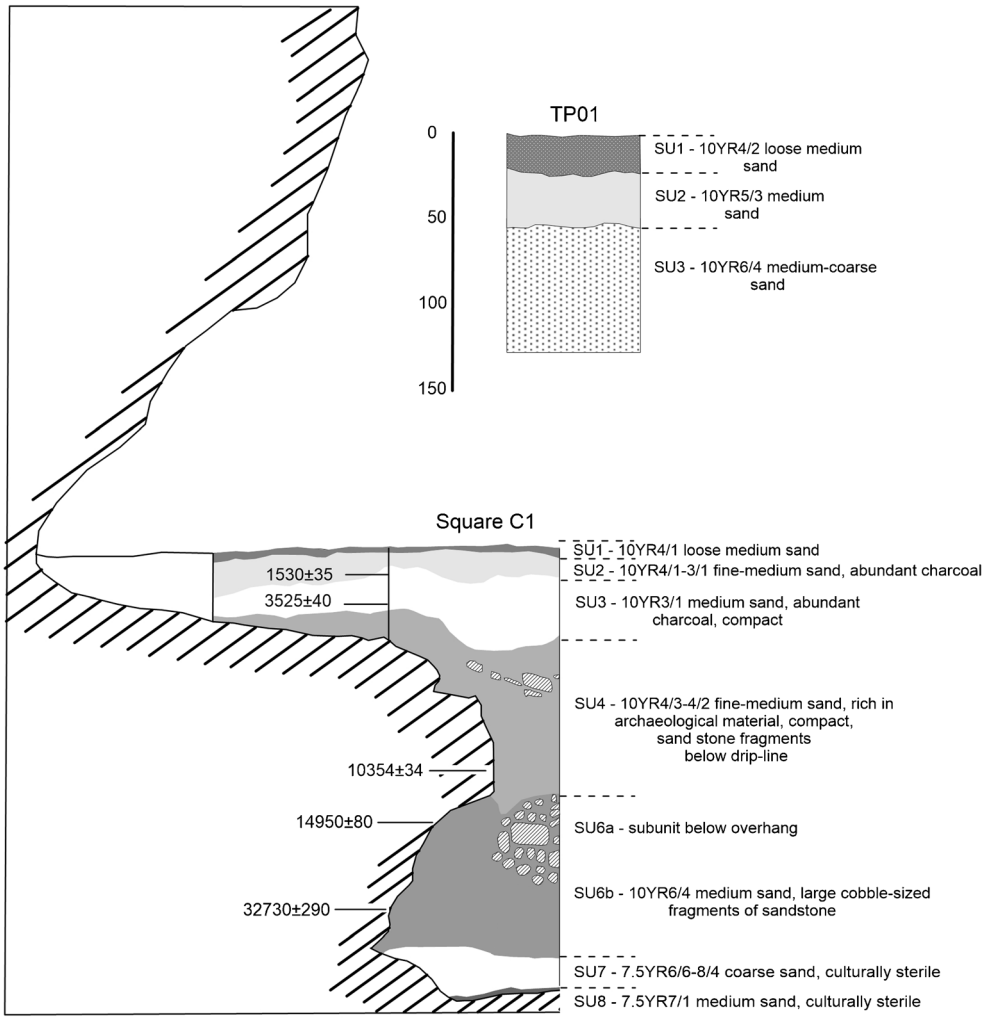

Fig. 4 Stratigraphic west wall section profiles of Squares D1, C1 and B1 (modified from Lowe et al. 2016)

μ-FTIR analyses were conducted directly on materials in the micromorphological samples using a Cary 660 FTIR microscope coupled to a Cary 670 bench (Agilent Technologies) housed at the University of Tübingen. Mid-IR spectra (4,000–400 cm^{-1}) were collected in transmission mode and in reflectance mode using a germanium crystal attenuated total reflectance (ATR) objective. Analytical areas were variable in transmission mode, with rectangular apertures ranging from ~200 × 200 μm to as small as ~20 × 20 μm, depending on the morphology of the target material. Circular analytical areas using the Ge-ATR were fixed at ~50 μm diameter. Transmission spectra were generated from 64 co-added scans at a resolution of 4 cm^{-1} with a background on glass and epoxy resin. Because glass and resin absorb strongly over much of the mid-IR spectral range, only peaks between 3,750 and 3,550 cm^{-1} were considered in this study. In general, this range limits μ-FTIR analyses to peaks associated with the OH-stretching region of clay minerals (Beauvais and Bertaux 2002; Robin et al. 2013). Ge-ATR spectra were generated from 32 co-added scans at a resolution of 4 cm^{-1} with backgrounds on air. Peaks associated with polyester resin were removed using the spectral subtraction function in the Resolutions Pro software package (Agilent Technologies). Relative to transmission spectra, reliable peaks were present in the Ge-ATR over a range of 4,000–570 cm^{-1}. Minerals were identified using a variety of digital search libraries (Downs 2006; Mentzer, personal collection; Weiner, S., personal communication), and published reference spectra (Chukanov 2013; van der Marel and Beutelspacher 1976).

Observations under OIL and reflected light, as well as the μ-FTIR analyses, focused on identification of iron-bearing minerals that contribute to the magnetic susceptibility of the sediments. Descriptive criteria and important IR peaks are listed in Table 4.

Magnetic susceptibility

Loose sediment samples were collected from every 5-cm layer in the archaeological test pits, and every 20 cm in the off-site test pits and were packed in small non-magnetic Althor P15

Table 1 Sedimentary description for GS1

Stratigraphic unit (SU)	Depth (cm)	Munsell colour	Texture	Sorting	Structure	pH	Other
Square C1							
SU1	0–5	Dark grey (10YR 4/1)	Loose, medium sand	Poorly to moderately sorted	Subangular	5	Few charcoal fragments and leaf litter
SU2	5–20	Dark grey to very dark grey (10YR 4/1–3/1)	Fine-medium sand	Poorly to moderately sorted	Subangular	5	Moderately compacted with small roots and holes. Charcoal is abundant. Sandstone rocks are present, but only in areas below the drip line.
SU3	20–50	Very dark grey (10YR 3/1)	Medium sand	Poorly sorted	Subangular	5	Abundant charcoal. Moderately compacted with small roots and holes. Sandstone rocks are present, but only in areas below the drip line.
SU4	50–155	Lower levels are brown (10YR 4/3) overlain by dark greyish brown (10YR 4/2)	Fine–medium sand	Poorly to moderately sorted	Subangular	5–5.5	Compacted, rich in archaeological material. Large quantities of sandstone rock fragments are present in areas below the drip line.
SU6a and b	155–232	Light yellowish brown (10YR 6/4)	Medium sand	Poorly sorted	Subangular	5–5.5	Subunit 6a is the area of deposit underneath the overhanging bedrock which contains only very small quantities of stone artifacts, while Subunit 6b is the area of deposit beyond the overhanging bedrock. Cobble-sized fragments of sandstone are present in Subunit 6b. The lower portion of SU6 is entirely culturally sterile.
SU7	232–250	Homogeneous reddish yellow (7.5YR 6/6) to pink (7.5YR 8/4)	Medium-coarse sand	Poorly sorted	Subangular	5.5	Culturally sterile, dry
SU8	250–260	Talc-like light grey (10YR 7/1)	Medium-coarse sand	Poorly sorted	Subangular	5	Culturally sterile, very thin

Table 2 Sedimentary description for TP01–TP04

Stratigraphic Unit (SU)	Depth (cm)		Munsell colour	Texture	Sorting	Structure	pH	Other
	TP01	TP02						
SU1	0–25	0–28	Dark greyish brown (10YR 4/2)	Fine to medium sand	Poorly to moderately sorted	Subangular	5	Few charcoal fragments on surface only, culturally sterile.
SU2	25–53	28–60	Brown (10YR 5/3)	Medium sand	Poorly to moderately sorted	Subangular	5	Culturally sterile, dry
SU3	53–120	60–120	Light yellowish brown (10YR 6/4)	Medium to coarse sand	Poorly sorted	Subangular	5.5	Culturally sterile, dry
	TP03	TP04						
SU1	0–30	0–30	Dark greyish brown (10YR 4/2)	Fine to medium sand	Poorly to moderately sorted	Subangular	5	Culturally sterile, dry
SU2	30–55	30–58	Greyish brown (10YR 5/2)	Medium sand	Poorly to moderately sorted	Subangular	5	Culturally sterile, dry
SU3	55–120	58–80	Pale brown (10YR 6/3)	Medium to coarse sand	Poorly sorted	Subangular	5.5	Culturally sterile, dry

boxes (5.28-cc volume). Sediment magnetic properties were measured in the laboratory using the Bartington Instruments' MS2B sensor. Low-field mass-normalized magnetic susceptibility (χ) readings at the maximum sensitivity were taken using both low (460 Hz) and high (4,600 Hz) frequencies for frequency dependence of susceptibility (χfd%). Frequency dependence is the difference between the measured low (χlf) and high (χhf) frequency and is often expressed as a percentage loss of the low frequency value ($\chi fd\% = (\chi 460Hz - \chi 4{,}600Hz/\chi 460Hz \times 100)$) (Dearing et al. 1996; Maher 1986). This measurement is used to show the contribution of ultrafine superparamagnetic (SP) grains (Dalan and Banerjee 1998; Dearing et al. 1996; Maher 1986). Increases in magnetic susceptibility in conjunction with χfd% potentially suggest an increase in the percentage of SP grains (Dearing et al. 1996), which are often found in burned or well-developed sediments.

These measurements were followed with anhysteretic remanent magnetization (ARM), saturation isothermal remanent magnetization (SIRM), hysteresis loops, and high- and low-temperature tests at the Institute for Rock Magnetism (IRM) at the University of Minnesota. Full details of ARM, SIRM, hysteresis loops and results are presented in Lowe et al. (2016). High-temperature (Curie point) and low-temperature analyses of the sediments were undertaken on 15 selected samples from the shelter, including from each stratigraphic unit except SU1 and SU8. The mineralogical transformations (e.g. oxidation of magnetite, dewatering of Fe-bearing clays) and temperature dependent magnetic transition (e.g. Verwey, Morin) observed during these measurements can improve our understanding of a sample's dominate magnetic mineral assemblage.

High temperature measurements were collected on a Geofyzika KLY-2 KappaBridge AC Susceptibility Bridge. Each sample was cycled to 600–650 °C to determine the Curie temperature, which allows the identification of specific magnetic minerals (Banerjee 1981; King et al. 1982; Thompson and Oldfield 1986). Curie temperatures were calculated using the first derivative of the susceptibility measurements (Lowe et al. 2016). Low-temperature measurements involved the examination of magnetic remanence of the samples as they were warmed and cooled. A Quantum Designs MPMS-5S (magnetic properties measurement system) was used, and an initial field of 2.5 T was applied before samples were measured. Samples were then cooled from room temperature (300 K) to 20 K and the remanence was measured at 5 K increments in a zero field. The samples were given another remanence in a field of 2.5 T at 20 K, and warmed from 20 up to 300 K, measuring remanence in a zero field at 5-K increments. The mineral magnetite cools through ~120 K and experiences a first-order phase transition called the 'Verwey transition,'

Table 3 Radiocarbon dates for GS1

Lab number	Square	Depth (cm)[a]	SU	^{14}C Age	±	Calibrated Age BP (95.4 % probability)
ANU-2625	C0	25	3	1,530	35	1,303–1,469
ANU-2629	C0	47	4	3,525	40	3,697–3,973
Wk-33293	B1	74	4	4,808	64	5,321–5,607
Wk-33294	B1	129	4	10,786	189	12,074–13,055
Wk-33296	C1	140	4	10,354	34	11,845–12,390
Wk-33292	B1	163	6b	14,464	235	16,915–18,160
Wk-33295	B1	168	6b	15,020	45	18,000–18,369
OZM095	C1	170	6a	14,950	80	17,904–18,350
OZM096	C1	175	6	22,180	130	26,017–26,738
OZM094	C1	205	6	32,730	290	35,992–37,764

[a] Depths are presented as centimetres below surface

where the mineral's crystalline symmetry changes from cubic to monoclinic.

Particle size, loss on ignition, phosphorous and FTIR

The dry sieving method of particle size analysis followed that of Ingram (1971) and McManus (1988) (for details see Keys 2009). Pre-treatment involved drying and weighing a10-g bulk sediment subsample from each 5-cm level. This was followed by ashing the samples for ~12 h in a muffle furnace at 450 °C to remove any organics and measure LOI values. Each sample was then screened through nested Endecotts sieves [1.00–500 μm (medium to coarse sand), 500–250 μm (fine sand), 250–125 μm (very fine sand) and <63 μm (silt and clay)] using a Geolab Systems mechanical sieve shaker.

Bulk sediment sub-samples for available P analyses were also taken from each 5-cm level, air-dried and sieved through a 2-mm-mesh sieve. Phosphorus extraction and measurement was done using a Mehlich 3 extraction technique (acetic acid, ammonium nitrate, ammonium fluoride and nitric acid; after Rayment and Lyons 2011, pp. 398–402) using a Varian Vista Port ICPOES (inductively coupled plasma optical emission spectrometry) instrument. Sample processing was undertaken at the University of Queensland.

Sieved subsamples of sediment collected from an off-site test pit were analysed for clay mineralogy using FTIR. The samples were analysed at the University of Tübingen using a portable bench FTIR equipped with a diamond crystal ATR accessory (Cary 630; Agilent Technologies). Spectra were produced from 32 co-added scans collected in the range of 4,000–450 cm^{-1} at a resolution of 4 cm^{-1}. Minerals were identified using digital and published reference spectra, as above.

Other parameters

All excavated materials recovered from the site were dry-sieved through 3- and 7-mm sieves. The 7-mm fraction was sorted in the field; the remaining 3-mm fraction was first floated in the laboratory for collection of all organic and botanical remains and then sorted. Stone artifacts and ochre were analysed noting raw material type, length, width and height. Other material collected included both the 7- and 3-mm fractions of charcoal, which were weighed and volumetrically corrected (for details see Carah 2010). The phytoliths were extracted by using an ashing technique (adapted from Bowdery 1998). Samples were first oven dried at 70 °C for 24 h and then sieved through a 1-mm mesh. Approximately ~7 g of sediment was place in lidded porcelain crucibles and weighed before being ashed in a muffle furnace at 450 °C for 24 h. The ashed material was first washed with hydrogen peroxide to remove any remaining organics, and then washed with hydrochloric acid to remove carbonates. The remaining phytoliths were dried and weighed.

Results

Micromorphology and μ-FTIR

In thin section, the GS1 sediments are dominated by sand-sized materials, with quartz being the most abundant mineral (Fig. 5a, b). Sand-sized fragments of accessory silicate minerals of sedimentary origin include microcrystalline quartz, weathered mica and hornblende, along with opaque grains, sand-sized aggregates of clay and quartz silt, with silica and oxyhydroxide mineral cements. Coarser materials include gravel-sized fragments of quartzite sandstone. Silt- and clay-sized materials are primarily present as coatings and bridges between quartz grains (Fig. 5c, d), although they also form rounded, sand-sized aggregates, sometimes associated with silt-sized fragments of charcoal and organic material. The mineralogy of the clay was studied using μ-FTIR measurements in transmission mode, and if possible, with the Ge ATR objective to obtain the entire

Table 4 Identification of magnetic and iron-bearing minerals at GS1

Mineral	Formula	Petrographic characteristics	Infrared spectra (transmission), bold indicates peaks that should be detectable using μ-FTIR	Infrared spectra (ATR), peak positions may shift to lower wavenumbers relative to transmission spectra	Magnetic parameters, Curie (T_C) or Néel(T_N) temperature and magnetic structure
Hematite	Fe_2O_3	Opaque under PPL, but with brown-red to yellow-red colours along edges or in thin areas. Orange to red under OIL and reflected light.	Bands at **635–647**, 531–545, 440–470 and 401 cm^{-1} (Chamritski and Burns 2005; Chukanov 2013; van der Marel and Beutelspacher 1976)	Bands at 515 and 438 cm^{-1} (RRUFF database; Downs 2006)	675 to –170 °C, Canted antiferromagnetic (Evans and Heller 2003; Hunt et al. 1995)
Goethite	α-FeO(OH)	Opaque under PPL, brown to yellow along edges or in thin areas. Yellow under OIL	Sharp bands are consistently present at **882–914** and **794–803** cm^{-1}, in addition to bands at **3,050–3,150, 660–667, 578–593** and 464–468 cm^{-1} that are variably present (Chukanov 2013; Prasad et al. 2006; van der Marel and Beutelspacher 1976)	The two main bands, are present, but shifted in position to **913–917** and **822**, with lesser peaks at **3,082, 686** and **587** cm^{-1} (RRUFF database; Downs 2006)	120 °C, Antiferromagnetic (Evans and Heller 2003; Hunt et al. 1995)
Lepidocrocite	γ-FeO(OH)	Opaque under PPL, can be red to yellow along edges or in thin areas.	Bands at **1,157–1,170, 1,018–1,020, 742–746**, 515–528 and 475–478 cm^{-1} (Chukanov 2013, van der Marel and Beutelspacher, 1976)	Bands at **1,159, 1,039** and **764** cm^{-1} (RRUFF database; Downs 2006)	–196 °C, Antiferromagnetic (Evans and Heller 2003; Hunt et al. 1995)
Magnetite	Fe_3O_4	Opaque under PPL. Grey to dark brown under OIL. Grey under reflected light.	One main band at **560–585** cm^{-1} (Chamritski and Burns, 2005; Chukanov 2013; van der Marel and Beutelspacher, 1976)	One band at 543–549 cm^{-1} (RRUFF database; Downs 2006)	578 to −155 °C, ferrimagnetic (Evans and Heller 2003; Maher and Taylor 1988)
Maghemite	γ-Fe_2O_3	Opaque under PPL.	Several bands in the range of 722–400 cm^{-1}, including sharp peaks at **635–638**, and 552–560 cm^{-1} (Chamritski and Burns 2005; Chukanov 2013; van der Marel and Beutelspacher 1976)	No available references	645 °C, ferrimagnetic (Evans and Heller 2003; Hunt et al. 1995)
Pyrite	FeS_2	Opaque under PPL. Brass yellow under OIL. Distinctive cubic morphology.	Band at 410–416 cm^{-1}, variably present; does not produce reliable peaks (van der Marel and Beutelspacher 1976)	Bands at **816–841** most prominent in two reference samples (RRUFF database; Downs 2006)	325 °C, Ferrimagnetic, antiferromagnetic (Evans and Heller 2003; Hunt et al. 1995)
Kaolinite, *with Fe^{3+} substitution for Al^{3+}	$Al_2Si_2O_5(OH)_4$	Colourless to red under PPL. Colourless under OIL.	In the OH-stretching region, **3,695, 3,668, 3,650** and **3,620** cm^{-1}, plus **3,595** cm^{-1} (Fe3+) (Beauvais and Bertaux 2002)		

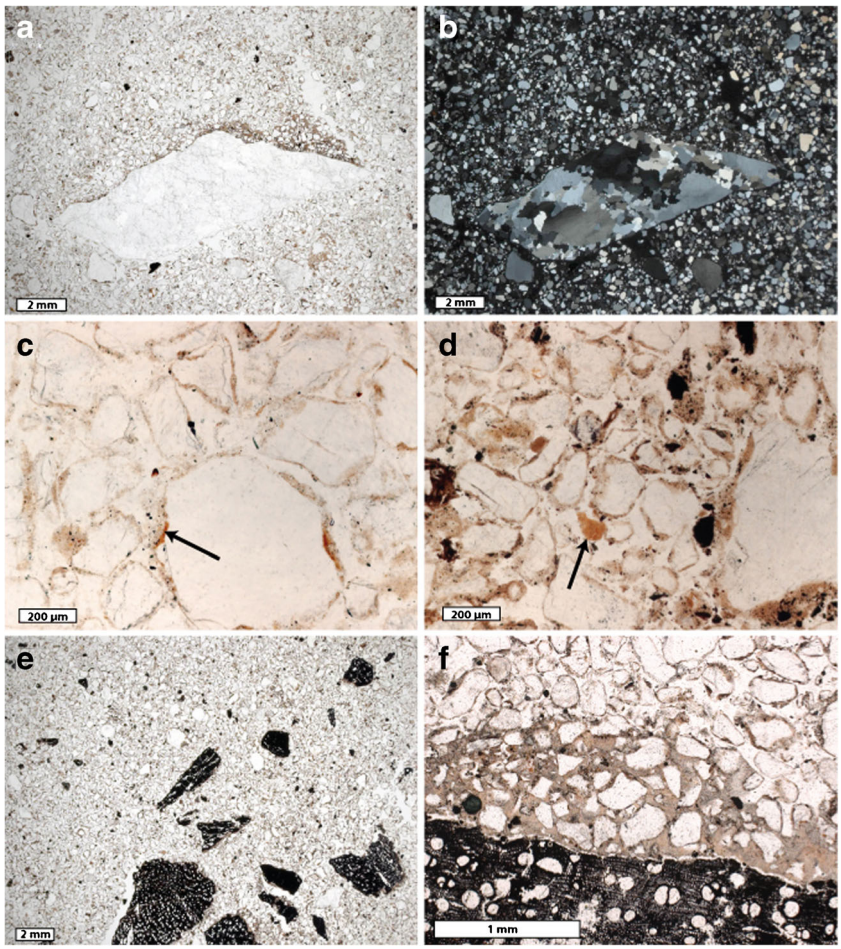

Fig. 5 The main geogenic sedimentary components and possible anthropogenic materials identified in thin section. **a** A sample from SU4 contains abundant sand-sized grains of quartz with packing and channel voids. A quartzite fragment is capped with silt and clay. PPL. **b** Same view as (**a**), XPL. **c** Quartz grains with thin coatings and bridges composed of clay with inclusions of organic material. One grain exhibits two phases of clay coating formation (*arrow*). PPL. **d** Quartz grains with thicker coatings and bridges composed of clay with inclusions of finely comminuted charcoal. A fragment of reddish clay coating (*papule*) is present in the fine sand fraction (*arrow*). PPL. **e** Large fragments of charcoal are present in the upper units of the sequence. PPL. **f** A fragment of charcoal is capped with a mixture of quartz sand, silt and pale brown clay. Crescentic coatings are visible. PPL

mid-IR spectrum (Fig. 6). Primary depositional fabrics, such as graded bedding or laminations, are generally absent and structural development is low throughout the entire sequence, with most samples exhibiting a massive structure. Anthropogenic materials seen in thin section include gravel- to silt-sized, angular to rounded charcoal

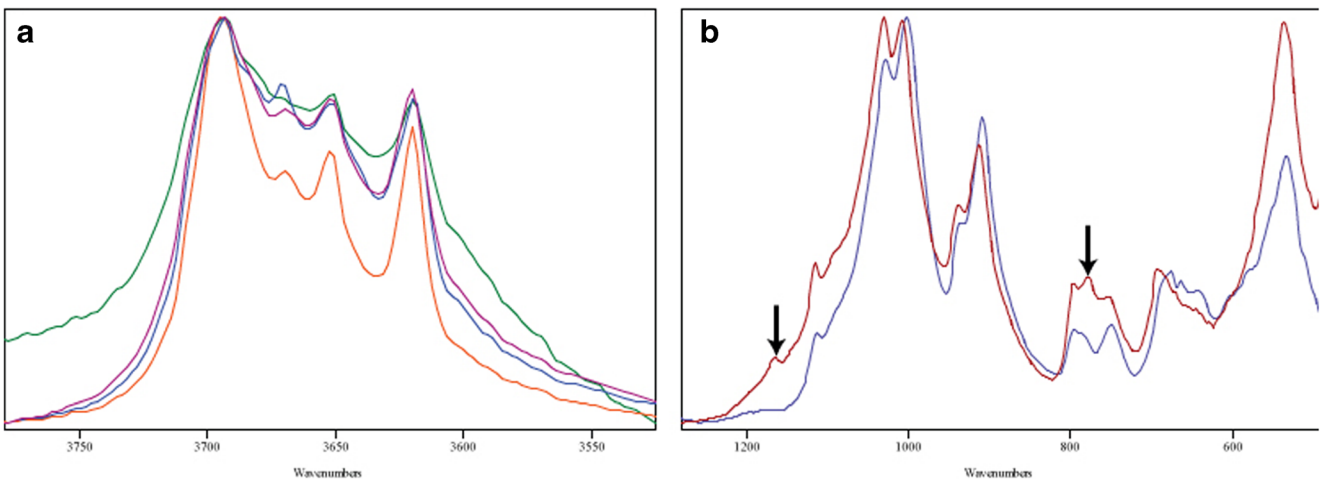

Fig. 6 FTIR spectra from the clay fraction of the sediment. **a** Transmission spectra collected using µ-FTIR on four different types of clay coatings and cappings (see Fig. 5). The peaks in the OH-stretching region are indicative of the mineral kaolinite. **b** ATR spectra of kaolinite. The blue spectrum was collected on a clay coating in thin section using the Ge-ATR objective. The *red spectrum* was collected on a loose sediment sample from a test pit located outside of the site using a diamond ATR. *Arrows* indicate peaks indicative of quartz

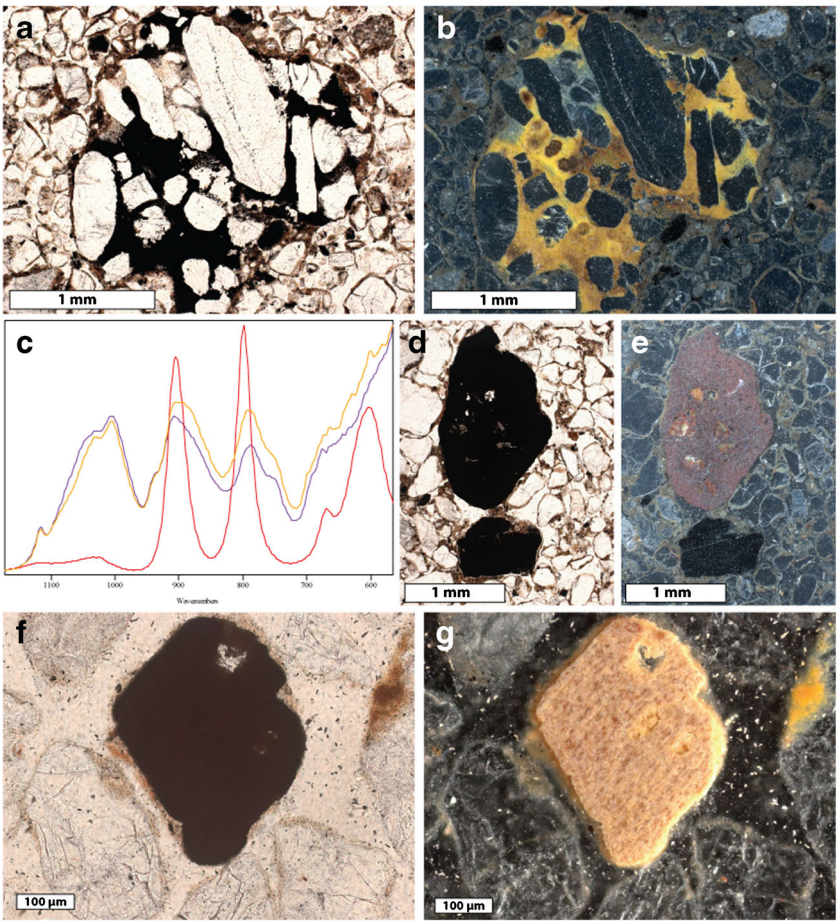

Fig. 7 Coarse opaque materials were identified using OIL and μ-FTIR. **a** A iron concretion fragment with quartz sand inclusions is present in SU4. PPL. **b** Under OIL, the cement is yellow, and additional inclusions are visible. **c** μ-FTIR analyses of the cement (*purple and yellow spectra*) indicate that it is composed of goethite. A reference spectrum for goethite is shown in red (S. Weiner, personal communication). **d** Two sand-sized opaque materials are visible in the SU4 sample. PPL. **e** The upper of the two grains is red under OIL and is likely composed of hematite. Kaolinite was also identified in this fine concretion using μ-FTIR. The lower opaque grain is charcoal. **f** A sand-sized opaque grain from SU6. PPL. **g** The grain is highly reflective under OIL with a striking pale yellow colour. Unfortunately, the μ-FTIR spectrum did not contain any peaks in the mid-IR region

fragments (Fig. 5e, f), as well as rare fragments non-local quartzite. Ash, phytoliths and bone fragments were not documented in any of the micromorphology samples.

In addition to red clay coatings on sand grains, potential iron-bearing materials are rare, but present throughout the sequence (Figs. 7 and 8). Sand- and gravel-sized concretions composed of sand-sized grains of quartz embedded in a dark red to opaque matrix (PPL) are present in six samples (Fig. 7a, b). OIL and reflected light analyses suggest that the cement is composed of a mixture of hematite and goethite. Goethite was positively identified in two concretions using μ-FTIR (Fig. 7c). Other iron-bearing materials are sand- and gravel-sized fragments of dark red to opaque material that contains silt-sized fragments of quartz (Fig. 7d, e). Both types of coarse concretions are interpreted as having formed elsewhere, due to the strong differences in texture, and when present, fabric of the included quartz relative to the surrounding sediment. The cement in these concretions frequently contains kaolinite. Both types of concretions are present throughout the sequence, and therefore it is impossible to distinguish between geogenic inputs and fragments of anthropogenic ochre.

Opaque grains are also present in the sand and silt fraction of the sediment (Fig. 7f, g). Many sand-sized opaque grains are strongly red in OIL, which suggests that they are composed of hematite (see Table 4). Similar microcrystalline hematite is present as a cement within some sandstone fragments (Fig. 8c, d), which suggests bedrock weathering may provide a natural source of hematite to the GS1 deposits. Hematite is also associated with decayed organic material. Other sand-sized opaque minerals are pale yellow in OIL and do not produce peaks in the mid-IR region (Fig. 7f, g). Opaque grains in the silt fraction are more variable in colour and morphology. Their presence as inclusions within quartz (Fig. 8a, b) and staining within other sand grains (Fig. 8e, f) suggests that the bedrock is one source of these minerals to the site. Rhombic, silt-sized minerals that are pale yellow in OIL are concentrated in sedimentary aggregates in SU7 and SU6 (see below). These minerals are present throughout the GS1 sequence as a component of the silt fraction. Although these minerals remain unidentified, they lack grey colour under reflected light and peaks in the mid-IR region. Thus, it is unlikely that these grains are magnetite, or maghemite, a strongly magnetic mineral (see Table 4). In total, iron-bearing minerals comprise less than 1 % of the sediment, and the majority of opaque grains in the GS1 deposits were identified as charcoal using OIL and reflected light (see Fig. 7d, e).

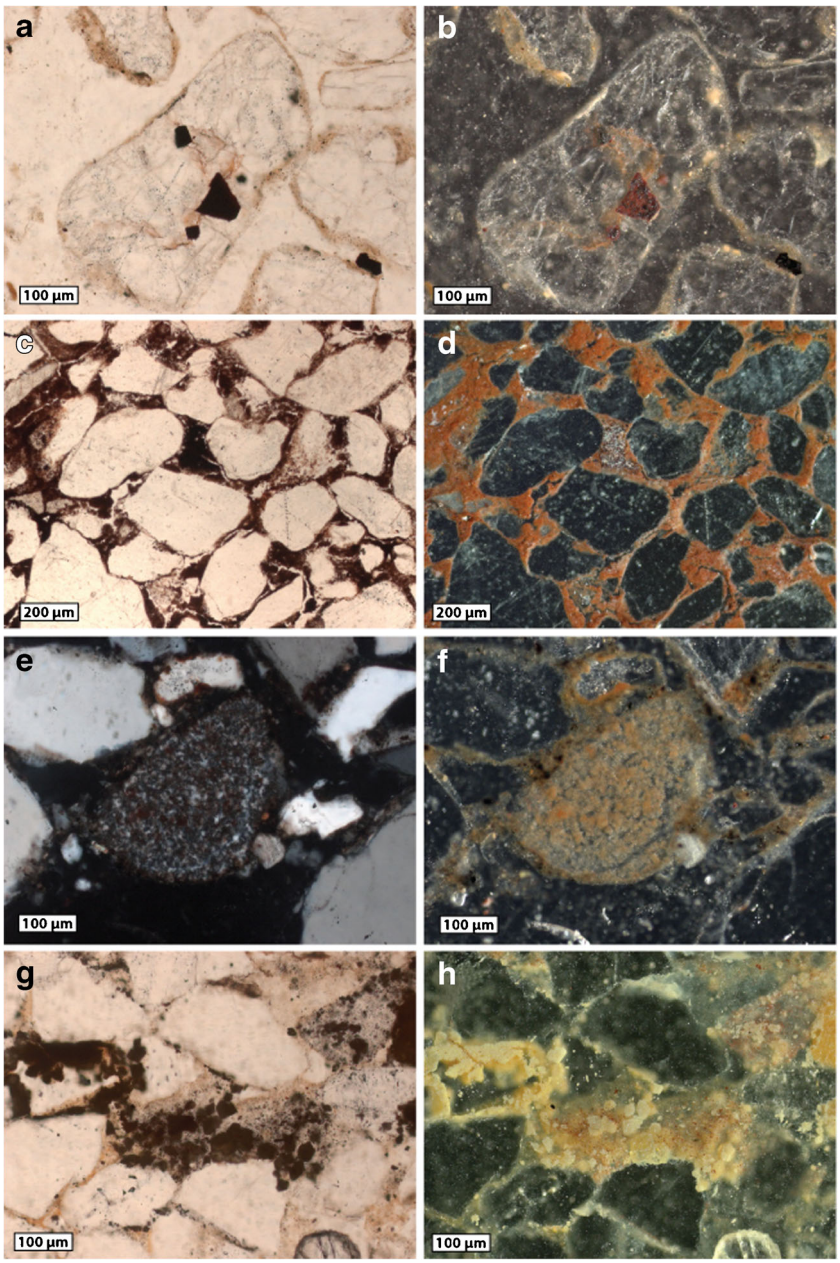

Fig. 8 Several different types of fine opaque materials were identified using OIL. **a** A sand grain contains opaque minerals. PPL. **b** The minerals are deep red under OIL. Similar minerals are rare but present in the silt fraction and likely source from the bedrock. μ-FTIR spectra on these minerals did not produce peaks in the mid-IR region. **c** A fragment of sandstone contains a cement that is dark red to opaque in PPL. **d** The cement is strongly red under OIL and is likely composed of hematite. **e** A sand-sized fragment of microcrystalline quartz contains diffuse red stain. XPL. **f** Under OIL, the red staining is orange to red and is likely composed of hematite. **g** A sediment aggregate from SU6 contains silt-sized grains of an opaque mineral with a characteristic rhombic morphology. PPL. **h** Under OIL, the grains are pale yellow in contrast to the reddish diffuse hematite below them. Similar grains are present throughout the sediments as a component of the silt fraction and inclusions in grain coatings. The mineral is presently unidentified. Less common cubic grains with brassy yellow colour under OIL are likely pyrite

Post-depositional features include tubular domains interpreted as infilled burrows, channel and chamber voids, fine sedimentary cappings on top of sand- and gravel-sized materials (see Fig. 5a, f), compound grain coatings (see Fig. 5c), and gravel-sized aggregates of sediment composed of sand-sized materials cemented or bound together with infillings of silt and clay. The vertical and lateral variation of primary geogenic and anthropogenic materials, structure and porosity, post-depositional features, and mineralogy of components identified using μ-FTIR are described in more detail below.

The SU7 and SU6 deposits are characterised by a massive grading to locally spongy microstructure composed of sand- and silt-sized grains of quartz separated by packing voids. The quartz grains within the matrix exhibit discontinuous thin coatings of orange to pale brown clay-sized material, identified using μ-FTIR as kaolinite (see Fig. 5c). Many coatings contain silt-sized inclusions of organic material. Gravel-sized aggregates containing sand-sized quartz grains, silt and clay are also present (Fig. 9). The fine sediment in the aggregates range in colour and texture from red moderately limpid clay, to yellow limpid clay microlaminated with quartz silt (Fig. 9a, b). Compound coatings at the centres of the aggregates contain red clay overlaid by yellow clay. In addition, the outer edges of the aggregates contain increased abundance of yellow clay and silt-sized inclusions, which suggests that the

fine sediment in these aggregates accumulated during at least two phases. Reflectance under OIL indicates that the red clay in the centres of the aggregates is rich in iron (Fig. 9c, d). μ-FTIR analyses indicate that the clay fraction of all types of infillings and coatings in these aggregates (red clay, yellow clay, and silty yellow clay) is composed of kaolinite. Some aggregates exhibit internal concentrations of iron oxides, which appear to be composed of hematite. Relative to the surrounding matrix, the aggregates contain sand-sized materials that exhibit a higher degree of textural sorting; accessory minerals such as biotite are also present. The sand, silt and clay aggregates are therefore interpreted as reworked, and may represent remnants of an older phase of sediment deposition within the shelter or external material sourced from a Bt horizon of a soil.

Although two micromorphology samples were collected across the boundary between SU7 and SU6, a discrete contact between them is not recognisable in thin section. Relative to SU7, SU6 is more porous due to the presence of channel voids, and contains a higher abundance of silt- and clay-sized materials coating and bridging between the spaces of the quartz grains within the matrix, as well as a lower abundance of sedimentary aggregates. Weak sedimentary laminations of coarse sand grains are present in SU6; however, this primary fabric is disrupted by the presence of infilled burrows. Sand-sized grains, and one gravel-sized fragment of fine iron concretion are present in the SU7 and SU6 samples. Anthropogenic materials are absent from both SU7 and lower portion of SU6.

SU6a is characterised by sand-sized grains of quartz that exhibit thin, discontinuous coatings of clay. Some coatings exhibit internal stratification, with interior layers of iron-rich red clay overlain by brownish clay. Both types of coatings are composed of kaolinite. The structure of this unit is massive, with packing voids between grains. Charcoal fragments are present, but very rare. A sandy iron concretion from this unit contains both hematite and goethite cement (see Fig. 7a, b, c). Tubular domains (in millimetre to centimetre scale) exhibiting slight textural differences relative to the surrounding sediment are likely infilled insect burrows.

As in other units, the sedimentary matrix of SU4 is dominated by sand-sized grains of quartz with an overall massive structure punctuated by occasional channel voids. The sand grains are typically coated with yellowish brown clay composed of kaolinite mixed with charcoal, although multi-component coatings containing an interior layer of iron-rich red clay—again, composed of kaolinite—are also present (see Figs. 5d and 10a). The abundance of fine material generally increases towards the top of the unit, within grain coatings and bridges, in zones of localised porphyric related distribution, and within sand-sized micro-aggregates (Fig. 10c). The overall fabric of SU4 is consistent with infilled channel voids and burrows (Fig. 10b), and the localised granular microstructure is suggestive of bioturbation. Charcoal abundance is variable, though most abundant at the top of the unit (see Fig. 5e), with fragments ranging from angular, gravel-sized pieces, to well-rounded fragments of sand-size, as well as silt-sized fragments within quartz grain coatings. The coarse materials in this unit, which include gravel-sized fragments of charcoal, exhibit cappings of fine sediment on their upper surfaces (see Fig. 5f). These cappings contain yellowish-brown clay composed of kaolinite and silt-sized fragments of charcoal. One sample contains a gravel-sized aggregate of sediment that is similar to those present in SU7 and SU6.

SU3 contains abundant sand-sized, well-rounded fragments of charcoal in a matrix of loose quartzitic sand. The sand grains are coated in fine sediment, with multicomponent coatings comprised of interior layers of yellowish brown clay and exterior layers composed of silt-sized fragments of charcoal and degraded organic material in a matrix of clay. μ-FTIR analyses indicate that the clay in each layer of these compound coatings is kaolinite. Sand-sized aggregates of quartz in a matrix of reddish to brownish clay are also present. These may be reworked soil aggregates. Fragments of degraded organic material are associated with secondary iron oxides that are red in OIL and possibly related to biomineralization. The overall fabric of the sample, like those from SU4, is consistent with infilled channel voids.

The single sample from SU2 contains intact sediment at its base, as well as an upper disturbed area that may contain sediment sourced from SU1 (Fig. 10d). The basal portion is very similar to the sediment that is present in SU3, with coated, sand-sized grains of quartz, and abundant fragments of charcoal, particularly within the sand fraction. Fragments of organic material and insect faecal pellets are also present. The upper portion is highly porous and contains abundant fragments of fresh to partially-humified organic material. The disturbed zone is rich in reworked aggregates of clay and silt.

Magnetic susceptibility

There is a positive correlation between the relative abundance of non-magnetic material such as wood charcoal, LOI and P with the magnetic susceptibility data (Fig. 11). In general, the susceptibility values increase at the position in the sequence where stone artifacts first occur (i.e. about 220 cm), and both susceptibility and χfd% remain consistently higher than those found in the lower, culturally sterile units. These increases in susceptibility result from organic matter, changed oxygen conditions and possibly increased fire use (see Lowe et al. 2016). Values are highest in the top portion of the sequence (SUs 3–1). Weakly magnetic samples are found in the culturally sterile layers (basal units of SU8, SU7 and lower SU6). The higher values in the top portion of the sequence also contrast considerably to those found in the off-site control test pits, which contained similar values to the culturally sterile sediments (see

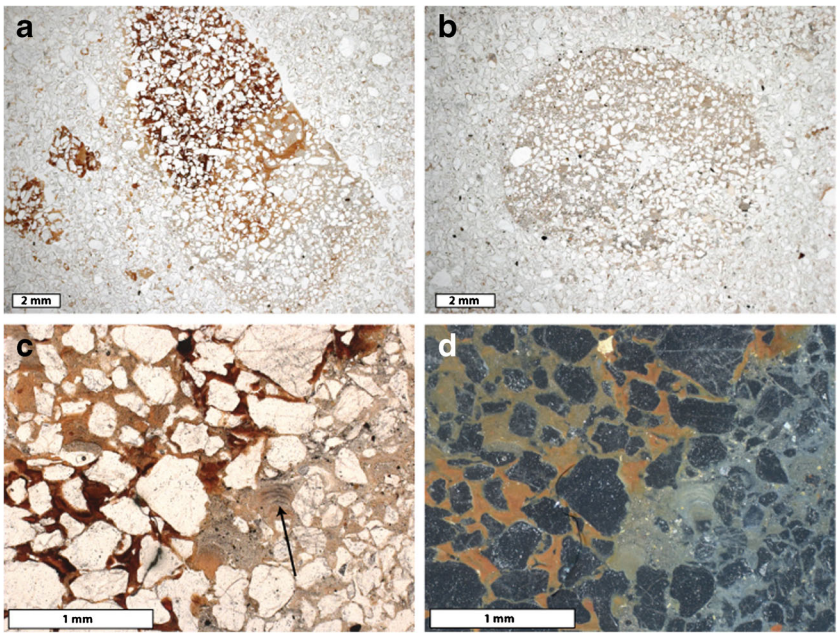

Fig. 9 Samples from SU7 and SU6 contain large aggregates of quartz sand, silt and clay. **a** The aggregates in SU7 contain fine materials that vary in colour and texture. Interior regions of the aggregates contain red clay overlain by yellowish clay. The exterior zones contain yellow clay mixed with quartz silt. The aggregates appear to be reworked from their original place of formation based on slight differences in the sand fraction mineralogy compared to the surrounding sediment, as well as sharp boundaries. Sand grains in the surrounding matrix are coated with clay and organic material (see Fig. 5c). **b** A strongly rounded aggregate from SU6 contains fine sediment with alternating broad horizontal bands of pale brown clay and silty clay. **c** Higher magnification view of different colours and textures of the fine sediment infillings. Crescentric infillings (*arrow*) indicate that the fine sediment was deposited by water, and that aggregates have been rotated during transport from their original place of formation. PPL. **d** Under OIL, the red clay is rich in hematite

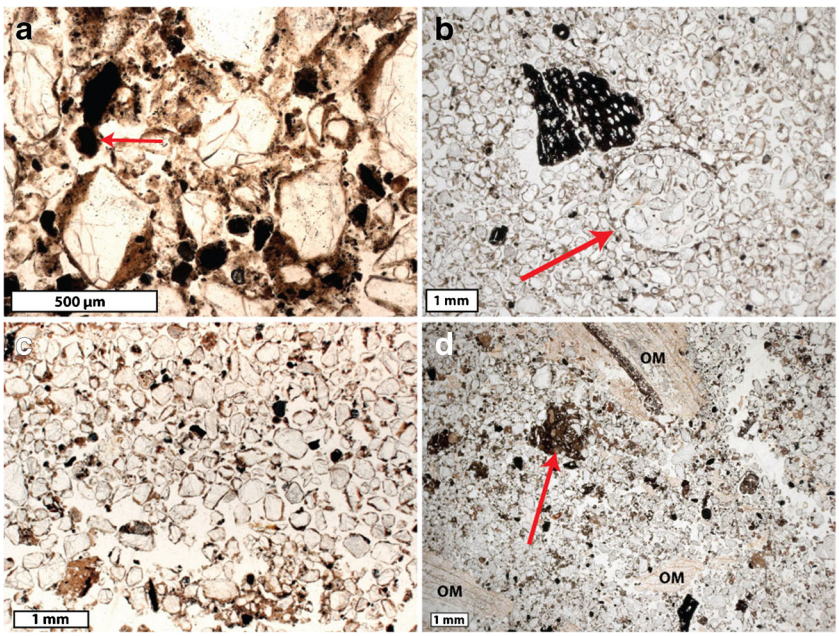

Fig. 10 Samples from the upper units contain abundant reworked anthropogenic materials. **a** In SU4, as well as in overlying SU3, charcoal is abundant in the sand- and silt-sized particle fraction. All opaque materials except one (*arrow*) in this image are charcoal. Silt-sized charcoal fragments are mixed with brown clay within the sand grain coatings. PPL. **b** Gravel-sized charcoal fragments are also abundant in the upper units. An infilled burrow (*arrow*) is evidence of insect bioturbation. PPL. **c** Samples from SU4 are rich in fine sediment, which locally fills the spaces between quartz sand. In places, the microstructure is granular with rounded sand-sized aggregates of fine sediment that likely formed as a result of bioturbation. **d** The uppermost sample contains a disturbed zone that may contain sediment from SU1. This zone contains large fragments of organic material (OM), and fragmented aggregates of silty clay. PPL

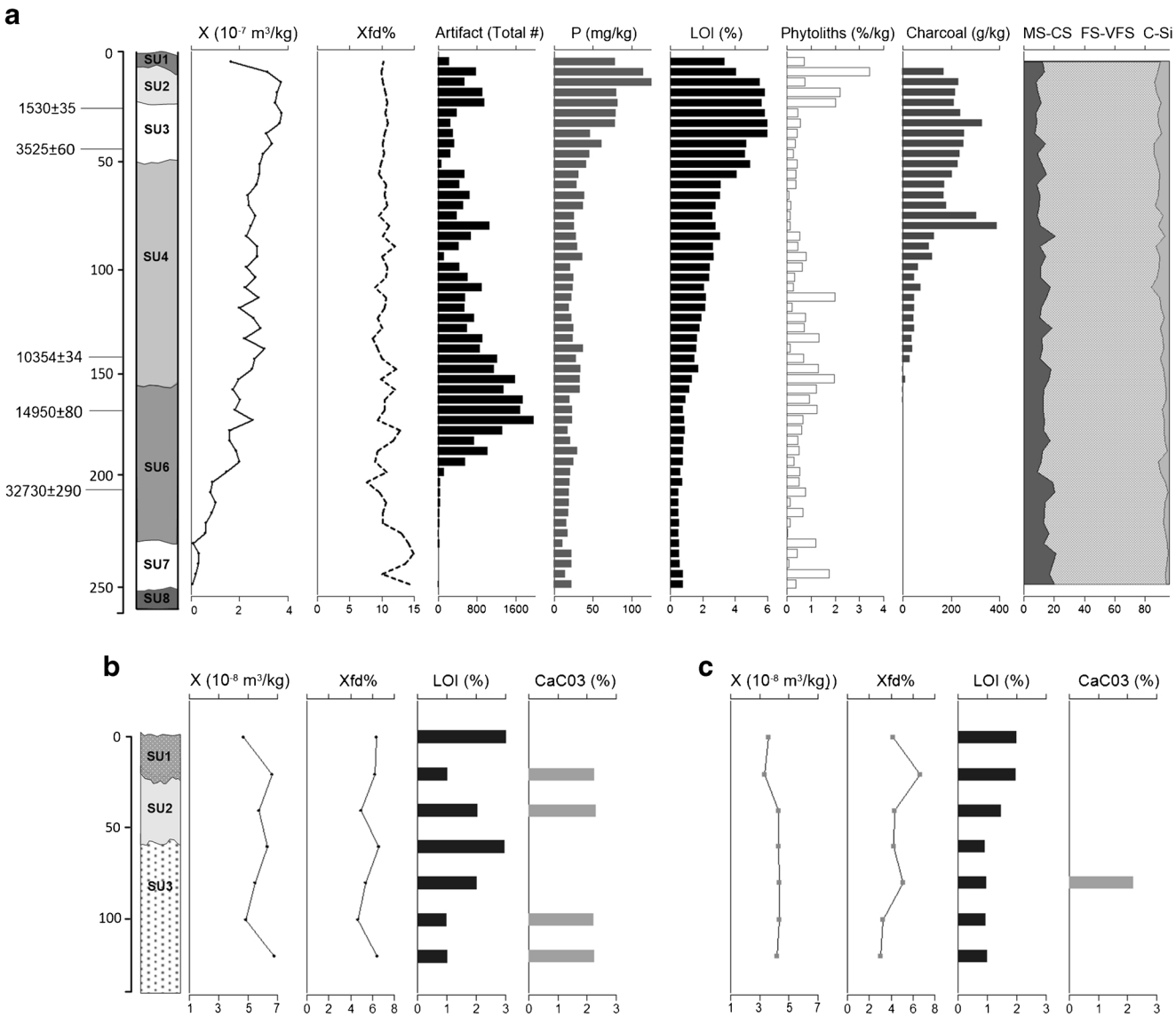

Fig. 11 Profile of low-field magnetic susceptibility and frequency dependence for Squares C1 (**a**) and (**b**) TP01 (*left*) and TP02 (*right*). Stratigraphic profile, stone artifact total, phosphorous, loss on ignition, phytolith weight percentage per gramme, charcoal, particle size and calcium carbonate data are also provided. Laboratory numbers for radiocarbon from top to bottom: ANU-2625, Wk-33293, Wk-33296, Wk-33295, OZM094. *MS* = medium sand, *CS* = coarse sand, *FS* = fine sand, *VFS* = very fine sand, *C* = clay and *Si* = silt

Lowe et al. 2016). The χfd% measurements range from 9 to 12 %, indicating that they contain a significant percentage of superparamagnetic grains. A bivariate plot of χ to mass-specific frequency-dependent susceptibility (χlf–χhf) shows a positive and linear relationship (Fig. 12), indicating a greater percentage of SP grains in the GS1 assemblage (Dearing et al. 1997; Jordanova et al. 2001).

High- and low-temperature magnetic measurements

The Curie temperatures (Tc) on measured samples ranged from 537 to 594 °C, with most samples having Tc <580 °C (Fig. 13). At least three varieties of magnetic phenomena were expressed in the data. The first magnetic behaviour is found in the uppermost portion of the stratigraphy and is defined by the susceptibility peaks near 300 °C during heating. This feature is most likely the inversion of maghemite to hematite. Maghemite is a metastable mineral phase that can display a range of Curie temperatures up to 640 °C (Liu et al. 2005; Özdemir and Banerjee 1984). The irreversible behaviour on cooling seen in Fig. 13a, c, shows that the final room temperature susceptibility is almost double the starting susceptibility for both samples and that new magnetic minerals were created during heating, likely partially oxidized magnetite (Tc = ~500–550 °C) as Fe-bearing clay minerals were dewatered. The same new magnetic minerals were also created in the sample shown in Fig. 13b, although at a lower concentration. This behaviour is not observed within the non-

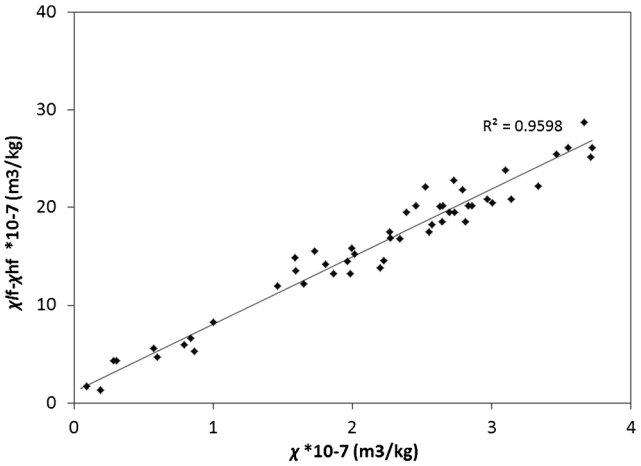

Fig. 12 Bivariate plot showing the relationships between χlf and χlf–χhf is positive and linear, suggesting a strong SP population

anthropogenic sediments near the bottom of the stratigraphy. The mineralogical transformations observed in SU3, SU2 and upper SU4 could result from the presence of paramagnetic minerals (i.e. Fe-bearing silicates or phyllosilicates) (Dunlop and Özdemir 1997) or other carbon-rich organic material (Dekkers 1990; Hanesch et al. 2006; Ketterings et al. 2000). Both charcoal and LOI are also higher in those upper units (top of SU4 and SUs 3–1), while SU6 has lower concentrations of organic-rich material and shows no mineral transformations.

The second magnetic behaviour reveals thermally stable magnetic mineral assemblages, where susceptibility curves are mostly reversible when cooled and exhibit a single ferrimagnetic phase. These samples contained Tc between 500–580 °C and were produced by samples located in the middle parts of the stratigraphy (upper SU6 to mid to lower SU4) (Fig. 13d–f). Minor amounts of new magnetic material were created at the end of these measurements, particularly in lower SU6 (Fig. 13g).

The third magnetic behaviour demonstrated extremely irreversible magnetic mineral assemblages and were found in SU7, in the culturally sterile basal units (Fig. 13h). These samples were very weakly magnetic and a large amount of magnetic material was produced during the cooling phase, so much that the final temperature susceptibility is four times larger than the initial room temperature susceptibility. High-temperature test of all samples measured indicated that they were oxidized magnetite.

Low-temperature SIRMs (LTSIRM) and room-temperature (RT) remanence measurements show how the samples vary during thermal cycling between 20 K and room temperature (Fig. 14a, c, e). The LTSIRM warming curves (solid line) show a loss of remanence on warming over the entire temperature range. Since there is little information that can be derived from this data, the RTSIRM cooling curves (dashed lines) have shown to be more useful in revealing inflection points near mineral transformations. A first-order transition called the 'Verwey transition' for the mineral magnetite as it cools through ~120 K is observed in all samples in the RTSIRM data. This is where the mineral's crystalline symmetry unblocks the nanoparticles of magnetite/maghemite (e.g. Hunt et al. 1995). The Verwey transition is not clearly visible in some of the curves shown (Fig. 14a, c, e); therefore in some units, the derivative curve is better for showing that slope changes near 120 K are likely related to this transition (Fig. 14b, d, f).

The mineral hematite experiences the 'Morin transition' an important magnetic transition from 200–260 K. As magnetic grain sizes decrease, the Morin transition is pushed towards these lower temperatures. The Morin transition is present in the uppermost stratigraphic layers (SUs, 4–2), but not in the lower layers (lower SU6 or SU7). This indicates that it is almost absent, and that the remanence is carried primarily by cation-deficient (maghemitized) and/or cation-substitute magnetite (see Lowe et al. 2016).

Particle size, loss on ignition, phosphorous and FTIR

Particle size analyses reveal the GS1 deposits are dominated by fine to very fine sand-sized grains (70–80 %), with small percentages of silt- and clay-sized material (<10 %) and medium- to coarse sand-sized material (5–15 %) (Fig. 4; see also Keys 2009). Silts and clays are more common in the upper portion of the sequence, decreasing slightly around 120 cm or below (i.e. mid-SU4). In turn, medium to coarse sands are less common near the surface of the sequence and increase slightly with depth. These results are consistent with the micromorphological analyses, which revealed the presence of multiple types of clay coatings and capping in the upper portion of the sequence, and a peak in fine sediment in the upper portion of SU4. Most sediments are poorly sorted, though tend to be more moderately sorted in the upper three SUs, and contain a mix of subangular particles. The uppermost SUs, 3–1, have the highest concentrations of P and LOI, the values for which both decrease with depth and are strongly correlated (Table 5 and Fig. 4). FTIR spectra of the clay fraction of loose sediment samples from off-site test pits (0–120 cm depth) indicate that the mineralogy is dominated by kaolinite (see Fig. 6b).

Other parameters

Wood charcoal quantities were also higher in the top of the sequence (SUs, 3–1) and correlate well with the increases in magnetic susceptibility in these units (see Fig. 11). Wood charcoal decreased significantly in the lower levels of SU4 and only a few fragments were preserved in SU6. Phytoliths were present throughout the GS1 deposits, in

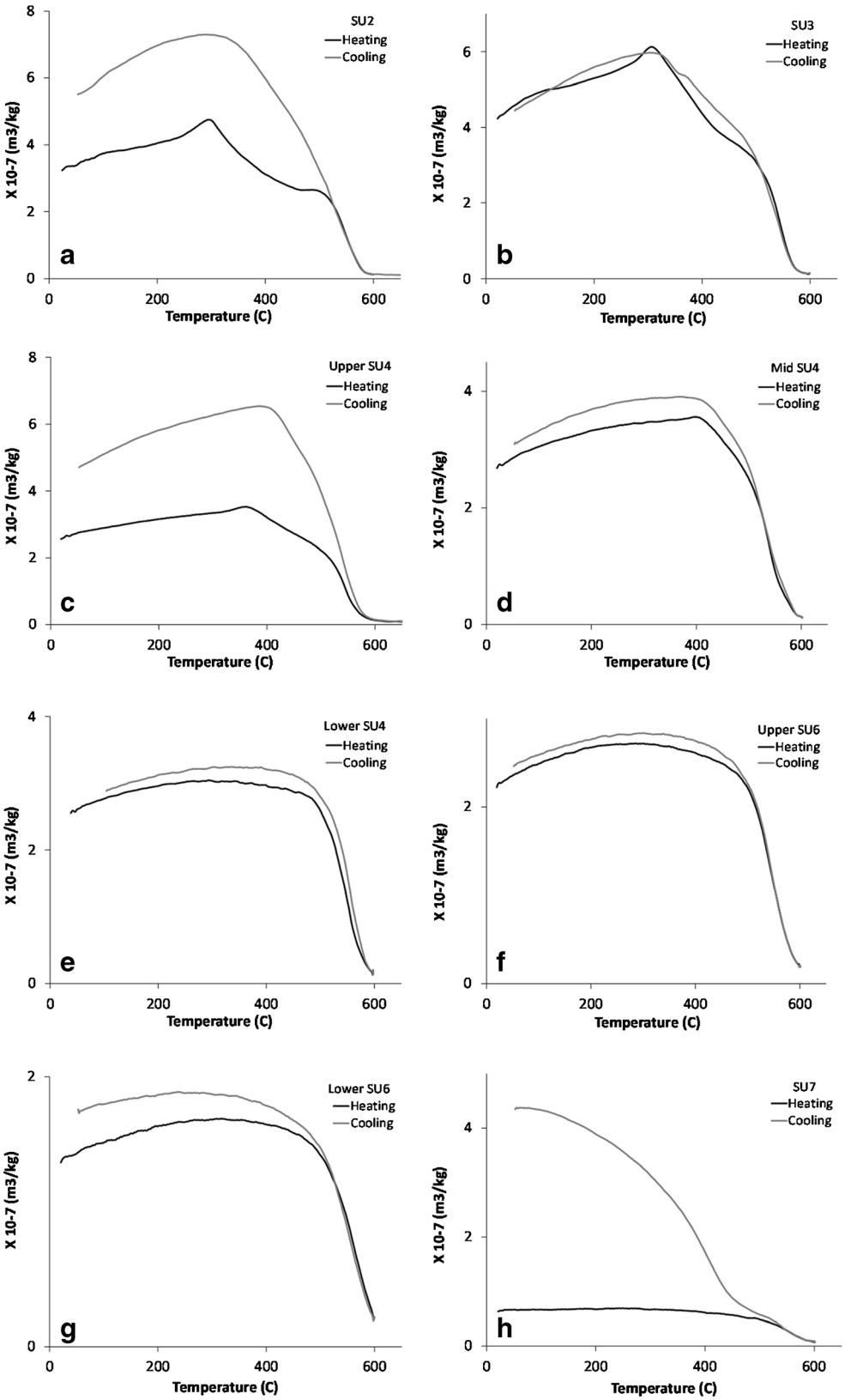

Fig. 13 High (Curie temperature) curves on selected samples of (**a**–**c**) irreversible curves and the production of a new magnetic mineral, probably magnetite, (**d**–**g**) reversible curves with only a minor amount of susceptibility created and (**h**) extremely irreversible curves and the production of a large amount of magnetic material

greatest abundance in SUs 2 and 1, with large quantities in SU6 (after the arrival of people) and in lower SU4. In upper SU4 and SU3, phytolith abundances were extremely limited. A light density of stone artifacts, mainly flakes,

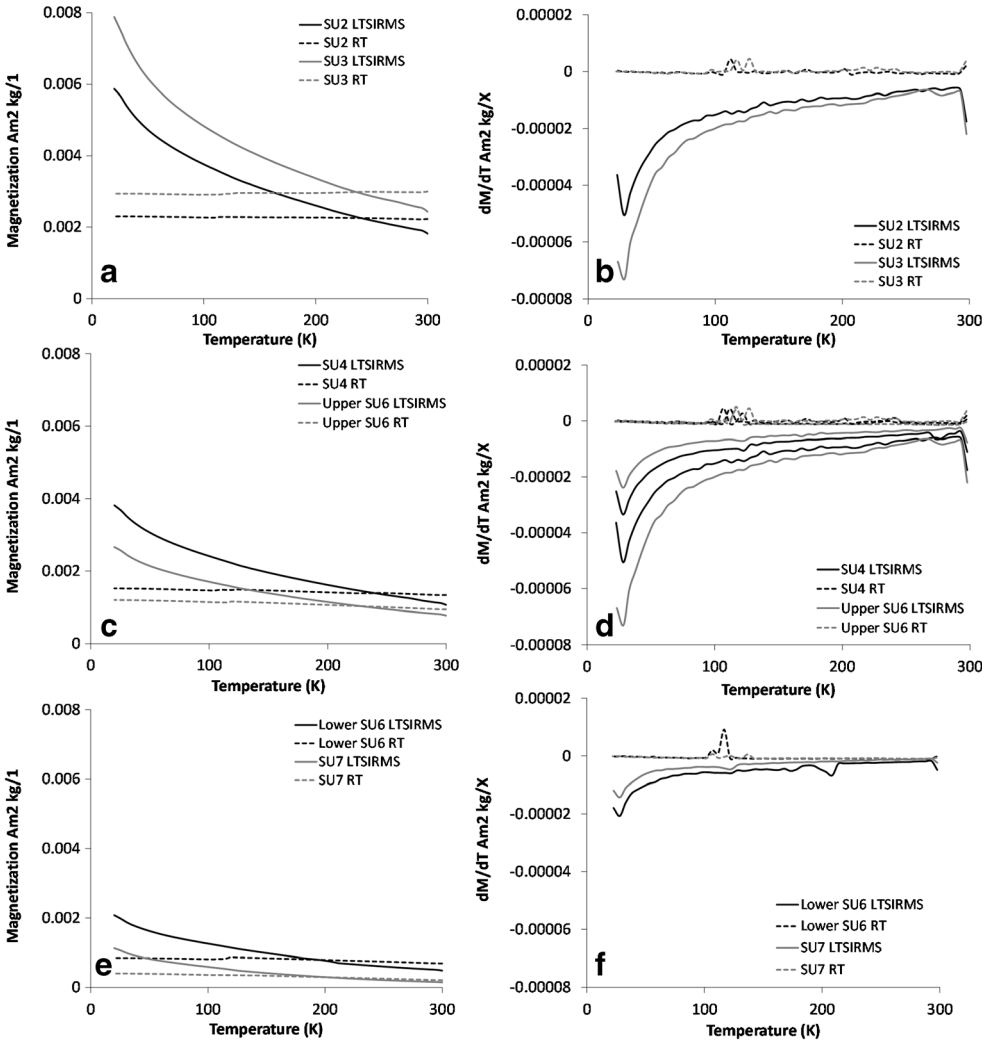

Fig. 14 Room-T SIRM measured while cooling in zero field, and low-T SIRM (LTSIRMS) measured while warming in zero field (**a** and **c**). All show only faint signs of the Verwey (**b** and **d**) and Morin transition (**a** and **b**)

first appears in the mid-lower portion of SU6, marking the initial onset of human occupation. Ochre is also present at this depth. Both stone artifacts and ochre become more abundant in the upper SU6 and throughout SU4, before declining in abundance in SU3 and then rising again in SU2. The stone artifacts are predominately flakes and cores of local raw materials including quartzite, quartz, chert and silcrete, with rare appearances of basalt, crystal quartz and chalcedony. The raw material types generally remain the same throughout the sequence although quartzite and silcrete disappear around SU3. Ochre also changes in SU3, yet not in abundance, but in the average size, becoming smaller with time. No charcoal or artifacts were observed in any of the off-site control test pits.

Table 5 Correlations between LOI (X) and Pav (Y)

Square	Line of best fit	R^2	Pearson's r
C1	$1{,}460.7x + 5.4266$	0.7996	0.8942
B1	$2{,}077.4x + 1.2543$	0.6502	0.8063
D1	$2{,}180.1x - 17.304$	0.9167	0.9574
D0	$3{,}400.6x - 34.182$	0.9181	0.9582
B0	$2{,}215.1x - 27.109$	0.6556	0.8097

Discussion

Each type of analysis conducted at GS1 provides information about the formation processes of the sedimentary sequence. We utilised a two-tiered approach to synthesizing the results, first integrating the micromorphology, μ-FTIR and magnetic susceptibly, and second, supporting aspects of the formation model with data drawn from the supplemental loose sediment analyses. Micromorphology provided context to magnetic susceptibility measurements, and both approaches characterised the anthropogenic sedimentary inputs. The resulting formation model helps refine the story of human occupation at the site.

Site formation processes

Our results indicate that accumulation of the sedimentary deposits in the GS1 site resulted from both natural and cultural processes. The majority of sandy sediment deposited is geogenic in origin, and likely sourced from roof fall and weathering of the local sandstone bedrock as evidenced by the granular disintegration and overall composition, texture and fabric of the sediments in thin section. The fine component of the sediment is dominated by clay, with some quartz silt. The mineralogy of the clay fraction is invariable throughout the sequence, despite differences in colour and texture of post-depositional sedimentary features. The ubiquitous presence of kaolinite both inside and outside the shelter suggests that clay mineralogy may be controlled by source. The depositional mechanism for the fine material within the shelter is unknown, as primary fabrics have been obliterated by bioturbation and much of the material has translocated downward through the profile. It is possible that some fine sediment entered the site in the form of soil aggregates.

Despite the relatively open nature of the site, there is little evidence of well-developed soil horizons throughout the sequence, a phenomenon observed on other sandstone rockshelters (see David et al. 2007). In contrast, the off-site test pits exposed sequences with visible boundaries between surface and subsurface horizons. We attribute the lack of horizons within the site to sediment mixing, low rates of pedogenesis, or both. In the upper stratigraphic units, organic materials show progressive decomposition with depth, consistent with only very weak soil formation at the modern ground surface. Buried surfaces and lag deposits were not observed in the field or in thin section.

Although wetting of the deposit is not occurring today (with excavated sediments between the shelter wall and dripline remaining dry even during extreme rainfall events), the micromorphological evidence indicates that water has played a role in shaping the GS1 deposits, at least in the pre-Holocene units. Thin sections revealed that fine material has translocated downward through the sequence, forming thin illuvial cappings and bridges on sand grains. Thicker silty clay cappings on gravel-sized materials, especially in the lower SUs are also evident in thin section, while crescentric coatings within some cappings indicate that some of the translocation was associated with the movement of water through the sequence. Coatings and features such as these can form rapidly (Rawling 2000) and can result from phases of increased precipitation (Birkeland 1999), localised dripping or water running along the shelter walls. Furthermore, bone and ashes are entirely absent from the sedimentary sequence, despite evidence for human occupation. With pH values ranging between 5 and 5.5, it is likely this absence is a result of preservation conditions (see David et al. 2007). We suggest that these materials may have dissolved when acidic waters seeped through the site (c.f. Canti 2003; Hedges and Millard 1995). Unfortunately, the micromorphological analyses cannot contribute to understanding the frequency of wetting events. The presence of compound coatings indicates that there were multiple phases of downward movement of materials in the GS1 deposits, the most recent of which mobilized anthropogenic materials in the form of finely comminuted charcoal.

Inputs of anthropogenic materials, including stone artifacts, charcoal and ochre are present from mid-SU6 and above, though absent in SU8, SU7 and the lower portion of SU6, and in all off-site control test pits. Within SU4, when it first appears preserved in the sequence, the overall abundance of charcoal, its distribution across various particle size classes, and the degree of rounding of individual fragments varies, with the coarsest and most abundant charcoal in the upper part of this unit. Above this, rounded, sand-sized fragments of charcoal are abundant in SU3 and SU2, where post-depositional disturbance is more visible, particularly in thin section. Discrete layers or lenses of charcoal are absent from the entire sequence, as are other hearth components that can be readily identified in thin section—when present—such as layers of ash or basal zones of heat-altered (reddened) substrate (cf. Mentzer 2014). Other macroscopic markers of burning within the shelter, such as burned bones or heated rock fragments, were not recovered. Microscopic materials, such as fragments of burned bone or calcareous ashes are also absent. The absence of anthropogenic sedimentary features associated with burning or otherwise, is likely due to dissolution under acidic conditions combined with syn- or post-depositional mixing by humans (e.g. scuffing and trampling), insects and larger fauna. Sandstone shelters that have little disturbance from mixing in Australia often contain stratigraphic features such as fire hearths and layers of distinctively textured sediment (Sullivan and Hughes 1983). These processes resulted in mechanical abrasion and lateral reworking of coarse charcoal fragments, and resulted also in finely comminuted charcoal as a component of the loose sediment and clay coatings, especially in SUs 4–1. The high temperature magnetic measurements confirm this.

Even with the geogenic nature of the sediment and a lack of combustion features, there is evidence for human modification of the deposits, provided primarily via the magnetic data. Clay minerals (alumina-silicates), oxides and hydroxides of iron and aluminium found within the shelter are major constituents of most sediments and rocks in northern and western Australian rockshelters. When they become fired, these minerals can be transformed to more strongly magnetic minerals by heating (Singh et al. 1991). Lowe et al. (2016) has shown that this transformation occurs within the shelter and that the increases in magnetic enhancement are produced by anthropogenic burning of wood fuel. The increased susceptibility in the sediments is a combined result of additional organic matter

(e.g. elevated P concentrations), changed oxygen conditions (e.g. elevated charcoal), and increased utility of fire (e.g. LOI). The significant population of SP-sized grains, the stable and consistently higher χfd% in the sediment and high and low-temperature experiments where oxidized magnetite is present in all samples, confirms this. Such observations were not observed in the off-site test pit profiles. The micromorphological observations are consistent with minimal pedogenesis, and provide no evidence of redox reactions that could impact the magnetic signals. However, we should note that the fabric and microstructure of the sediment in thin section, as well as the rounding of the charcoal fragments, are consistent with post-depositional mixing geogenic and anthropogenic materials. This process led to centimetre-scale homogenization of the magnetic signals and precludes the possibility of using magnetic susceptibility to identify discrete heated surfaces in the site.

Although there is evidence of weathering, the variations in the magnetic susceptibility data and presence of artifactual material indicate that anthropogenic processes dominate the sedimentary sequence and as such, are more relevant for understanding the accumulation of sediment within the site than the record for environmental change. This is supported in the off-site control test pits which show different magnetic signatures, an absence of cultural material and definable horizons. Paleoenvironmental studies have shown pedogenic formation of ferrimagnetic minerals during wetting/drying cycles occur in caves and rockshelters that are favourable to these conditions (Ellwood et al. 1997; Herries 2006; Maher 1998), particularly those that are limestone. Sites containing arid or acidic soils, such as those found at GS1 often display little pedogenic enhancement (Bailey and Woodward 1997; Maher 1998). The absence of soil horizons throughout the sequence indicates that deposits were affected by weathering (dissolution) and lateral reworking of material (i.e. post-depositional mixing). The stable χfd% and magnetic susceptibility values found throughout the sequence after the onset of human occupation support this, as we would expect to see trends in the sequence if environmental factors were more dominant (see Ellwood et al. 1997). With the exception of localised biomineralization of hematite around decaying organic material, all of the observed and identified iron-bearing minerals in thin section are primary components of the bedrock or soil aggregates.

Integrative approach: strengths and weaknesses

In this study, we explored the potential for integration of micromorphology, in situ microanalyses and magnetic susceptibility in an old cratonic sandstone rockshelter in northern Australia. Relative to caves, rockshelters are exposed to more open conditions (cf. Herries 2009), and any interpretations of magnetic susceptibility data must consider post-depositional chemical alterations, including typical pedogenic processes, as well as the potential effects of sediment mixing.

As outlined in Table 4, several iron-bearing minerals that are relevant to magnetic susceptibility measurements are potentially present in the GS1 sediments. All are difficult to identify in micromorphological thin sections using transmitted light. Analyses under OIL and basic reflected light proved most useful in this study to distinguish between silt-sized opaque minerals such as hematite and goethite, and silt-sized fragments of charcoal (see Fig. 7). These analyses revealed that in SU4 and above, the majority of silt-sized opaque grains in the Gledswood sediments were derived from charcoal. A minority of opaque grains were derived from other minerals. Of these, most were gravel-sized fragments of material that could be interpreted as ochre or externally sourced geogenic concretions. More accurate identification of iron-bearing minerals in thin section would require quantitative reflected light analyses on polished mounts (e.g. Craig et al. 1981).

OIL analyses aided in the identification of hematite, which could not be observed in the high temperature magnetic measurements due to the sample's altering at temperatures >650 °C. Microcrystalline hematite was visible within the sandstone and is also apparent within the sand- and silt-sized particle fractions of the sedimentary deposits. Several of the fine coatings visible on grains in thin section contain kaolinite clays that are rich in iron, as evidenced by their strong red colours. The absence of a peak at 3,595 cm^{-1} in the FTIR transmission spectra of these (and all other) clays indicates that structural iron is not present within the kaolinite at this site (Beauvais and Bertaux 2002). We suggest that the red colour is instead due to staining by iron oxides. Of these materials, the silt-sized particles of microcrystalline hematite, the reddish clays, and the unidentified rhombic opaque grains (see Fig. 8g, h) appear to be most mobile throughout the sequence, as they are frequent components of grain coatings and cappings in the lower units.

μ-FTIR analyses were most useful for describing the mineralogy clay-sized particle fraction of the GS1 sediments. Although better methods exist for the identification of clay minerals (e.g. x-ray diffraction; Moore and Reynolds 1989), μ-FTIR presents an advantage in that analyses can be conducted in situ, which allows the analyst to document clay minerals forming from individual minerals within rocks or soils (Beauvais and Bertaux 2002; Robin et al. 2013), or stratigraphic variability in multicomponent clay coatings. The latter features were present in the GS1 thin sections; however, μ-FTIR analyses revealed only one clay mineral at the site: kaolinite (see Fig. 6). The μ-FTIR results also indicate that Fe^{3+} substitution is not present in any of the kaolinite at the site, and that colour variations in the clay coatings at the site—which range from brown to red to pale yellow—are due to staining by iron oxides and inclusions of microcharcoal and organic material.

μ-FTIR analyses did not prove to be very useful for the identification of opaque minerals in the GS1 sediments, with the exception of three positive identifications of the mineral goethite in sandy concretions (see Fig. 7c). We know from the high and low-temperature experiments that strongly magnetic phases, such as maghemite and magnetite, overwhelm much of the GS1 samples, but they were not identified in thin section. This method had limited success for several reasons. First, μ-FTIR measurements may only be conducted in a portion of the mid-IR region. Many iron oxide minerals, such as hematite, do not produce peaks in this region (see Table 4). Furthermore, poorly ordered phases may not produce peaks at all. The second reason for limited success of the μ-FTIR analyses is that the majority of the opaque materials within the site—including the materials that we suspect contribute most strongly to the magnetic signal—are silt-sized or smaller. In the region of interest for identifying iron oxides (<1,200 cm^{-1}; see Table 4), the measurement area is limited by the spot size of the Ge-ATR objective. Nevertheless, we feel that conducting in situ μ-FTIR measurements with the aim of aiding in the interpretation of magnetic susceptibility measurements may be a worthwhile approach at other types of sites, and recommend further exploration of this avenue of research with additional analytical approaches, such as microscopic X-ray diffraction or microscopic Mössbauer spectroscopy.

The strongest aspect of integration of the micromorphology, μ-FTIR and magnetic susceptibility proved to be the contributions of the former to reconstructing general post-depositional processes at the site. The micromorphological analyses revealed little evidence for pedogenic processes that could cause enhancements to the magnetic signals, and therefore supported the assertion that the strong magnetism is a proxy for burning.

Further implications for archaeology

The depositional sequence in GS1 commenced sometime prior to 40,000 years ago and was followed by the appearance of stone artifacts indicating occupation by people around 36,000–37,700 cal. BP (Wallis et al. 2014). After humans started utilising the site, modifications to the natural sedimentary sequence commenced, with a strongly positive correlation between the initial incorporation of discarded artifacts and an increase in magnetic susceptibility.

Stone artifacts, ground ochre fragments and wood charcoal are present throughout the sequence from mid-SU6 and above, with no indication for a cultural or temporal hiatus, unlike many other Pleistocene sandstone shelters in Sahul (cf. David et al. 1997; O'Connor et al. 1999). Based on the chronological, archaeological and geoarchaeological data, it appears that GS1 was occupied from ca 38,000 cal. BP, through and beyond the LGM. The presence of stone artifacts indicates that tool manufacture using locally available quartzite, quartz and chert, with some rare appearances of basalt, crystal quartz and chalcedony. Quartzite and silcrete began disappearing from the lithic assemblage in the mid-Holocene, suggesting a reorganisation of people or human activity in the landscape at that time. While it is possible to interpret the ground ochre as a proxy for the production of rock art, it is also conceivable that the ochre was being ground for some other purpose (such as body art or decoration of ceremonial or secular portable artifacts). As is the case with the stone artifact assemblage (see Wallis et al. 2014), there are also important changes in the Holocene portion of the sequence with regard to the ochre; not only does this material decline in abundance, but the average size of ochre fragments also decreases by about 50 % of that in the Late Pleistocene.

While no bone or hearths were observed in the excavations or in thin section, the mineral magnetic and charcoal data indicate that the occupants were using fire in the site, a similar phenomenon to that observed in limestone rockshelters in Greece (Bailey and Woodward 1997; Woodward and Bailey 2000). The absence of bone and other materials such as ash is likely due to dissolution, trampling, wind winnowing and possible intentional removal (i.e. rake out after use) (see David et al. 2007). The difference in grain size between the fragments of charcoal and the sedimentary components of the sequence could indicate transport mechanisms. In thin section, the charcoal-rich sediment is inconsistent with documented fire deposits (e.g. French et al. 2009). Furthermore, since hearths burn for longer durations and at higher temperatures, and require a significant amount of wood fuel compared to natural fires, the increases in magnetic enhancement, and results of temperature tests are consistent with the sediments at GS1 being predominantly the result of anthropogenic burning rather than natural bushfires (Lowe et al. 2016).

Finally, the organics and *P* values are also good indicators for human occupation at GS1, and both correlate positively to the artifactual and magnetic susceptibility data. Correlations between LOI, wood charcoal and P to the stone artifacts are less positive and likely indicate that human occupation is related to the extent as which these sediments are altered. Organic and available *P* values double after the LGM through to the mid-Holocene and continue to rise more markedly in the uppermost units. While organic matter can decrease rapidly with depth in a sequence due to a lack of biota living in the upper soil horizons (Bettis 1988; Holliday 1988), the dissolution combined with syn- or post-depositional mixing by humans, insects and larger fauna may have also had a

large effect on this reduction in the late LGM and early Holocene deposits.

Conclusion

The Gledswood Shelter 1 formed as a result of local input mechanisms related to the natural weathering of the Mesozoic sandstone bedrock and roof fall. As the shelter evolved, particularly around 38,000 cal. BP, a new agent began to influence sedimentation in the site: people. The presence of people was apparent not only from the stone artifacts they deposited, but from the increases in magnetic susceptibility caused by the magnetic modifications to the sediment. The micromorphology and magnetic susceptibility analyses did not reveal evidence of soil horizons nor discrete boundaries between stratigraphic units, and no buried surfaces or breaks in occupation identified. Post-depositional mixing by humans and insects, and weathering of materials further resulted in the abrasion and reworking of coarser material, such as charcoal, in the cultural units.

Despite the absence of hearths in the GS1 deposits, opening up the possibility that the charcoal present may have been the result of natural bush-fires, the mineralogical and magnetic susceptibility data confirm human activity in this site and this rather acidic environment is excellent at preserving these records. Micromorphological studies confirmed the presence of microcharcoal in thin section, even in the lower cultural units where macroscopic evidence of charcoal or burning was entirely absent. While the micromorphology identified the presence of iron-bearing minerals, particularly microcrystalline hematite and goethite, high and low temperature magnetic susceptibility tests were necessary to identify the presence of other fine-grained minerals including oxidized magnetite. While neither the magnetic susceptibility nor particle size data showed the distribution of these magnetic minerals in fine detail, or revealed whether they had been impacted by post-depositional processes, this information was apparent from the micromorphology data.

Finally, the resultant dataset has highlighted the benefit of using a mix of proxies for understanding old cratonic sandstone settings. Not only is the first time this has been applied in Australia, this study has shown another way to investigate light density sites. This is an important contribution to the study of Australian archaeology, specifically on sites that had only previously studied the stone artifact assemblage.

Acknowledgements We thank Kathryn Fitzsimmons in the Department of Human Evolution at the Max Planck Institute for Evolutionary Anthropology undertook the OSL dating, the results of which will be presented elsewhere. David Appleton in the School of Agriculture and Food Science at The University of Queensland carried out the processing of phosphorous samples and Josh Feinberg, Mike Jackson and Dario Bilardello from the Institute for Rock Magnetism, University of Minnesota, assisted with the magnetic analysis. Stewart Fallon, Ben Keys, Xavier Carah, Claire St George, Chantal Wight, Lydia McKenzie, Dan Rosendahl and Ian Moffat have been involved with various other aspects of the research and are thanked for their contribution to the wider project. We also thank the Woolgar Valley Aboriginal Corporation for supporting this research, including participation during fieldwork, and Flinders University, the Australian Institute of Nuclear Science and the Australian Institute of Aboriginal and Torres Strait Islander Studies for funding the research. We would like to acknowledge the generosity and hard work of the RRUFF project and Steve Weiner for making digital reference FTIR spectra available open access. Finally, we thank Jim Allen and Paul Goldberg for earlier comments on the manuscript in addition to James Woodward and one anonymous reviewer. KML was funded by the Institute of Rock Magnetism, University of Minnesota Visiting Research Fellowship and the University of Queensland, through an International Postgraduate Research Scholarship and Centennial Scholarship, and a Graduate School International Travel Award. Funding for μFTIR was provided by the Deutsche Forschungsgemeinschaft (MI 1748/3-1).

References

Abbott JT (1997) Stratigraphy and Geoarchaeology of the Red Canyon Rockshelter, Cross County, Wyoming. Geoarchaeology 12(4):315–335

Ajas A, Bertran P, Lemée L, Queffelec A (2013) Stratigraphy and palaeopedology of the Palaeolithic cave site of Combe-Saunière, southwest France. Geoarchaeology 28:432–449

Allen MJ, Macphail RI (1987) Micromorphology and magnetic susceptibility studies: their combined role in interpreting archaeological soils and sediments. In: Federoff N, Bresson LM, Courty MA (eds) Soil micromorphology. Plaisir/l'Association Francaise pour l'Etude du Sol, Pairs, pp 669–676

Allen J, O'Connell JF (2014) Both half right: updating the evidence for dating first human arrivals in Sahul. Aust Archaeol 79:86–108

Bailey G (2007) Time perspectives, palimpsests and the archaeology of time. J Anthropol Archaeol 26:198–223

Bailey GN, Woodward JC (1997) The Klithi deposits: sedimentology, stratigraphy and chronology. In: Bailey GN (ed) Klithi: Palaeolithic Settlement and Quaternary Landscapes in Northwest Greece, vol 1, Excavation and Intra-Site Analysis at Klithi. McDonald Institute for Archaeological Research, Cambridge, pp 61–94

Banerjea RY, Bell M, Matthews W, Brown A (2013) Applications of micromorphology to understanding activity areas and site formation processes in experimental hut floors. Archaeological and Anthropological Sciences 7(1):89–112

Banerjee SK (1981) Experimental methods of rock magnetism and paleomagnetism. In: Saltzman B (ed) Advances in geophysics, vol 23. Academic Press, New York, pp 25–99

Bazylinski DA, Moskowitz BM (1997) Microbial biomineralization of magnetic iron minerals; microbiology, magnetism and environmental significance. Rev Mineral Geochem 35(1):181–223

Beauvais A, Bertaux J (2002) In situ characterization and differentiation of kaolinites in lateritic weathering profiles using infrared microspectroscopy. Clay Clay Miner 50(3):314–330

Bettis EA (1988) Pedogenesis in late Prehistoric Indian mounds, upper Mississippi valley. Phys Geogr 9:263–279

Bird MI, Turney CSM, Fifield LK, Jones R, Ayliffe LK, Palmer A, Cresswell R, Robertson S (2002) Radiocarbon analysis of teh early archaeological site of Nauwalabila I, Arnhem Land, Australia: implications for sample suitability and stratigraphic integrity. Quat Sci Rev 21:1061–1075

Birkeland PW (1999) Soils and Geomorphology. Oxford University Press, New York

Bowdery D (1998) Phytolith analysis applied to Pleistocene-Holocene archaeological sites in the Australian arid zone, BAR International Monograph Series 695. Hadrian Books, Oxford

Bowdler S (1977) The coastal colonisation of Australia. In: Allen J, Golson J, Jones R (eds) Sunda and Sahul: prehistoric studies in Southeast Asia Melanesia and Australia. Academic Press, London and New York, pp 205–246

Bowler JM, Price DM (1998) Luminescence dates and stratigraphic analyses at Lake Mungo: review and new perspectives. Archaeol Ocean 33:156–168

Bronk Ramsey C, Dee M, Lee S, Nakagawa T, Staff R (2010) Developments in the calibration and modelling of radiocarbon dates. Radiocarbon 52(3):953–961

Bureau of Meteorology (2013) Monthly mean maximum temperature: Richmond Post Office. [Online]. Commonwealth of Australia, Melbourne. Available: http://www.bom.gov.au/climate/averages/tables/cw_030045.shtml Accessed 31 Jan 2013.

Canti MG (2003) Aspects of the chemical and microscopic characteristics of plant ashes found in archaeological soils. Catena 54(3):339–361

Carah X (2010) Corridors and callitris: examining the changing use of environment through the Gledswood Shelter 1 wood charcoal assemblage. School of Social Science, The University of Queensland, St Lucia, Unpublished BA(Hons) Thesis

Chamritski I, Burns G (2005) Infrared and Raman-active phonons of magnetite, maghemite and hematite: a computer simulation and spectroscopic study. J Phys Chem B 109(11):4965–4968

Chukanov NV (2013) Infrared spectra of mineral species: extended library., Springer Science and Business Media

Clarkson C, Smith M, Marwick B, Fullagar R, Wallis LA, Faulkner P, Manne T, Hayes E, Roberts RG, Jacobs Z, Carah X, Lowe KM, Matthews J, Florin SA (2015) The archaeology, chronology and stratigraphy of Madjedbebe (Malakununja II): A site in northern Australia with early occupation. J Hum Evol 83:46–64

Craig JR, Vaughan DJ, Hagni RD (1981) Ore microscopy and ore petrography (vol. 406). Wiley, New York

Dalan RA, Banerjee SK (1998) Solving archaeological problems using techniques of soil magnetism. Geoarchaeology 13:3–36

David B, Roberts RG, Tuniz C, Jones R, Head J (1997) New optical and radiocarbon dates from Ngarrabullgan Cave, a Pleistocene archaeological site in Australia: implications for the comparability of time clocks and for the colonization of Australia. Antiquity 71:183–188

David B, Roberts RG, Magee J, Mialanes J, Turney C, Bird M, White C, Fifield LK, Tibby J (2007) Sediment mixing at Nonda Rock: investigations of stratigraphic integrity at an early archaeological site in northern Australia and implications for the human colonization of the continent. J Quat Sci 22:449–479

Davidson I, Sutton SA, Gale SJ (1993) The human occupation of Cuckadoo 1 rockshelter, northwest Central Queensand. In: Smith MA, Spriggs M, Fankhauser B (eds) Sahul in review: Pleistocene Archaeology in Australia, New Guinea and Island Melanesia. Department of Prehistory, Research School of Pacific and Asian Studies, The Australian National University, Canberra, pp 164–172

Dearing JA, Hay KL, Baban SMJ, Hudleston SA, Wellington EMH, Loveland PJ (1996) Magnetic susceptibility of soil: an evaluation of conflicting theories using a national data set. Geophysics Journal International 127:728–734

Dearing JA, Bird PM, Dann RJL, Benjamin SF (1997) Secondary ferrimagnetic minerals in Welsh soils: a comparison of mineral magnetic detection methods and implications form mineral formation. Geophys J Int 130:727–736

Dekkers MJ (1990) Magnetic properties of natural goethite—III: magnetic behaviour and properties of minerals originating from geothite dehydration during thermal demagnetization. Geophysics Journal International 103:233–250

Derbyshire E, Kemp R, Meng X (1995) Variations in loess and palaeosol properties as indicators of palaeoclimatic gradients across the Loess Plateau of north China. Quat Sci Rev 14(7):681–697

Dockrill SJ, Simpson IA (1994) The identification of prehistoric anthropogenic soils in the Northern Isles using an integrated sampling methodology. Archaeol Prospect 1(2):75–92

Downs RT (2006) The RRUFF Project: an integrated study of the chemistry, crystallography, raman and infrared spectroscopy of minerals. Program and Abstracts of the 19th General Meeting of the International Mineralogical Association in Kobe, Japan

Ellwood BB, Petruso KM, Harrold FB, Schuldenrein J (1997) High-resolution paleoclimatic trends for the Holocene identified using magnetic susceptibility data from archaeological excavations in caves. J Archaeol Sci 24:569–573

Ellwood B, Harrold FB, Benoist SL, Thacker P, Otte M, Bonjean D, Long GJ, Shahin AM, Hermann RP, Grandjean F (2004) Magnetic susceptibility applied as an age-depth-climate relative dating technique using sediments from Scladina Cave, a late Pleistocene cave site in Belgium. J Archaeol Sci 31:283–293

Evans ME, Heller F (2003) Environmental magnetism: principles and applications of enviromagnetics. Academic Press, London

Farrand WR (1975) Sediment analysis of a prehistoric rockshelter: the Abri Pataud. Quatern Res 5:1–26

Farrand WR (2001) Sediments and stratigraphy in rockshelters and caves: a personal perspective on principles and pragmatics. Geoarchaeology 16:537–557

Fassbinder JWE, Stanjekt H, Vali H (1990) Occurrence of magnetic bacteria in soil. Nature 343(6254):161–163

Fifield LK, Bird MI, Turney CSM, Hausladen PA, Santos GM, di Tada ML (2001) Radiocarbon dating of the human occupation of Australia prior to 40 ka BP—success and pitfalls. Radiocarbon 43:1139–1145

French C, Periman R, Cummings LS, Hall S, Goodman-Elgar M, Boreham J (2009) Holocene alluvial sequences, cumulic soils and fire signatures in the middle Rio Puerco Basin at Guadalupe Ruin, New Mexico. Geoarchaeology 24(5):638–676

Ghiorse WC, Ehrlich HL (1992) Microbial biomineralization of iron and manganese. Catena, Supplement (21):75–99

Gifford-Gonzalez DP, Damrosch DB, Damrosch DR, Pryor J, Thunen RL (1985) The third dimension in site structure: an experiment in trampling and vertical dispersal. Am Antiq 50:803–818

Goldberg P, Berna F (2010) Micromorphology and context. Quat Int 214(1):56–62

Goldberg P, Macphail R (2006) Practical and theoretical geoarchaeology. Blackwell Publishing, Oxford

Goldberg P, Sherwood SC (2006) Deciphering human prehistory through the geoarcheological study of cave sediments. Evolutionary Anthropology: Issues, News and Reviews 15(1):20–36

Hanesch M, Stanjek H, Petersen N (2006) Thermomagnetic measuresments of soil iron minerals: the role of organic carbon. Geophys J Int 165:53–61

Hedges RE, Millard AR (1995) Bones and groundwater: towards the modelling of diagenetic processes. J Archaeol Sci 22(2):155–164

Herries AIR (2006) Archaeomagnetic evidence for climate change at Sibudu cave. South African Humanities 18:131–147

Herries AIR (2009) New approaches for integrating palaeomagnetic and mineral magnetic methods to answer archaeological and geological questions on Stone Age sites. In: Fairbairn A, O'Conner S, Marwick B (eds) New directions in archaeological science. The Australian National University Press, Canberra, pp 235–253

Herries AIR, Fisher EC (2010) Multidimensional GIS modeling of magnetic mineralogy as a proxy for fire use and spatial patterning:

evidence from the Middle Stone Age bearing sea cave of Pinnacle Point 13B (Western Cape, South Africa). J Hum Evol 59:306–320
Hiscock P (1988) Prehistoric settlement patterns and artefact manufacture at Lawn Hill, Northwest Queensland. School of Social Science, The University of Queensland, St Lucia, Unpublished PhD thesis
Hiscock P (2008) Archaeology of ancient Australia. Routledge Taylor and Francis Group, London
Hogg AG, Hua Q, Blackwell PG, Niu M, Buck CE, Guilderson TP, Heaton TJ, Palmer JG, Reimer PJ, Reimer RW, Turney CSM, Zimmerman SRH (2013) SHCal13 southern hemisphere calibration, 0–50,000 years cal. BP. Radiocarbon 55(4):1889–1903
Holliday VT (1988) Genesis of a late Holocene soil chronosequence at the Lubbock Lake archaeological site, Texas. Ann Assoc Am Geogr 78:594–610
Hughes PJ, Lampert RJ (1977) Occupational disturbance and types of archaeological deposit. J Archaeol Sci 4:135–140
Hunt CP, Banerjee SK, Han J-M, Solheid PA, Oches EA, Sun W-W, Liu T-S (1995) Rock-magnetic proxies of climate change in the loess-paleosol sequences of the western Loess Plateau of China. Geophys J Int 123:232–244
Ingram RL (1971) Sieve analysis. In: Carver RE (ed) Procedures in sedimentary petrology. Wiley-Interscience, New York, pp 49–69
Jordanova N, Petrovsky E, Kovacheva M, Jordanova D (2001) Factors determining magnetic enhancement of burnt clay from archaeological sites. J Archaeol Sci 28:1137–1148
Ketterings QM, Bigham JM, Laperche V (2000) Changes in soil mineraology and texture caused by slash-and-burn fires in Sumatra, Indonesia. Soil Science of American Journal 64:1108–1117
Keys BO (2009) Engrained in the past: using geoarchaeology to understand site formation processes at the Gledswood Shelter 1 Site, Northwest Queensland. University of Flinders, Adelaide, Unpublished BArch (Honors) thesis
King JW, Banerjee SK, Marvin J, Özdemir Ö (1982) A comparison of different magnetic methods for determining the relative grain size of magnetite in natural materials: some results in lake sediments. Earth Planet Sci Lett 59:404–419
Kooistra MJ, Pulleman MM (2010) Features related to faunal activity. In: Stoops G, Marcelino V, Mees F (eds) Interpretation of micromorphological features of soils and regoliths. Elsevier, Amsterdam, pp 397–418
Kovda I, Mermut AR (2010) Vertic features. In: Stoops G, Marcelino V, Mees F (eds) Interpretation of micromorphological features of soils and regoliths. Elsevier, Amsterdam, pp 109–127
Lamb L (1996) Investigating changing stone technologies, site use and occupational intensities at Fern Cave, north Queensland. Aust Archaeol 42:1–7
Le Borgne E (1960) Influence de feu sur les proprietes magnetiques du sol et sur celles du schist et du grantie. Ann Geophys 16:159–195
Lindbo DL, Stolt MH, Vepraskas MJ (2010) Redoximorphic features. In: Stoops G, Marcelino M, Mees F (eds) Interpretation of micromorphological features of soils and regoliths. Elsevier, Amsterdam, pp 129–147
Linford N, Linford P, Platzman E (2005) Dating environmental change using magnetic bacteria in archaeological soils from the upper Thames Valley, UK. J Archaeol Sci 32(7):1037–1043
Liu QS, Deng C, Yu Y, Torrent J, Jackson MJ, Banerjee SK, Zhu R (2005) Temperature dependence of magnetic susceptibility in Argon environment: implications for pedogenesis of Chinese loess/paleosols. Geophys J Int 161(1):102–112
Lowe KM, Shulmeister J, Feinber JM, Manne T, Wallis LA, Welsh K (2016) Using soil magnetic properties to determine the onset of Pleistocene human settlement at Gledswood Shelter 1, northern Australia. Geoarchaeology 31:211–228
Maher BA (1986) Characterisation of soils by mineral magnetic measurements. Physics of the Earth and Planetary Interior 42:76–92
Maher BA (1998) Magnetic properties of modern soils and Quaternary loessic paleosols: Paleoclimatic implications. Palaeogeography, Paleoclimatology, Palaeoecology 137:25–54
Maher BA, Taylor RM (1988) Formation of ultrafine-grained magnetite in soils. Nature 336:368–371
Marmet E, Bina M, Fedoroff N, Tabbagh A (1999) Relationships between human activity and the magnetic properties of soils: a case study in the medieval site of Roissy-en-France. Archaeol Prospect 6:161–170
Marwick B (2002) Milly's Cave: evidence for human occupation of the inland Pilbara during the Last Glacial Maximum. In: Ulm SC, Westcott C, Reid J, Ross A, Lilley I, Prangnell J, Kirkwood L (eds) Barries, borders, boundaries: Proceedings of the 2001 Australian Archaeological Association Annual Conference, Tempus 7. Anthropology Musem, The Univeristy of Queensland, St Lucia, pp 21–33
Marwick B (2005) Element concentrations and magnetic susceptibility of anthrosols: indicators of prehistoric human occupation in the inland Pilbara, Western Australia. J Archaeol Sci 32:1357–1368
McManus J (1988) Grain size determination and interpretation. In: Tucker ME (ed) Techniques in sedimentology. Blackwell, Oxford, pp 63–85
Mentzer SM (2014) Microarchaeological approaches to the identification and interpretation of combustion features in prehistoric archaeological sites. Journal of Archaeological Method and Theory 21(3):616–668
Mentzer SM, Quade J (2013) Compositional and isotopic analytical methods in archaeological micromorphology. Geoarchaeology 28(1):87–97
Miller CE, Conard NJ, Goldberg P, Berna F (2009) Dumping, sweeping and trampling: experimental micromorphological analysis of anthropogenically modified combustion features. P@lethnologie 2009: 25–37
Moore DM, Reynolds RC (1989) X-ray diffraction and the identification and analysis of clay minerals (vol. 378). Oxford University Press, Oxford
Morse K, Cameron R, Reynen W (2014) A tale of three caves: new dates for Pleistocene occupation in the inland Pilbara. Aust Archaeol 79: 167–178
Nielsen AE (1991) Trampling the archaeological record: an experimental study. Am Antiq 56:483–503
O'Connell JF, Allen J (2004) Dating the colonization of Sahul (Pleistocene Australia–New Guinea): a review of recent research. J Archaeol Sci 31:835–853
O'Connor S, Veth P, Barham A (1999) Cultural versus natural explanations for lacunae in Aboriginal occupation deposits in northern Australia. Quat Int 59:61–70
Özdemir Ö, Banerjee SK (1984) High temperature stability of maghemite (γ-Fe_2O_3). Geophys Res Lett 11:161–164
Prasad PSR, Prasad KS, Chaitanya VK, Babu EVSSK, Sreedhar B, Murthy SR (2006) In situ FTIR on the dehydration of natural goethite. J Asian Earth Sci 27(4):503–511
Rawling JE (2000) A review of lamellae. Geomorphology 35(1):1–9
Rayment GE, Lyons DJ (2011) Soil chemical methods—Australasia. CSIRO Publishing, Collingwood
Richardson N (1992) Conjoin sets and stratigraphic integrity in a sandstone rockshelter: Kenniff Cave (Queensland, Australia). Antiquity 66:408–418
Richardson N (1996) Seeing is believing: a graphical illustration of the vertical and horizontal distribution of conjoined artefacts using DesignCAD 3D. In: Ulm S, Lilley I, Ross A (eds) Australian Archaeology '95: Proceedings of the 1995 Australian Archaeological Association Annual Conference, Tempus 6. Anthropology Museum, Department of Anthropology and Sociology, University of Queensland, St Lucia, pp 81–95

Robin V, Petit S, Beaufort D, Prêt D (2013) Mapping kaolinite and dickite in sandstone thin sections using infrared microspectroscopy. Clay Clay Miner 61(2):141–151

Roebroeks W, Villa P (2011) On the earliest evidence for habitual use of fire in Europe. Proc Natl Acad Sci 108(13):5209–5214

Rosendahl D, Lowe KM, Wallis LA, Ulm S (2014) Integrating geoarchaeology and magnetic susceptibility at three shell mounds: a pilot study from the Gulf of Carpentaria, Australia. J Archaeol Sci 49:21–32

Singh B, O'Connor S, Veth P, Gilkes R (1991) Detection of amorphous alumino-silicate by x-ray diffraction and chemical analysis to detect firing in archaeological sediments. Archaeol Ocean 26(1):17–20

Smart J (1973) Gilberton, Queensland 1:250,000 Geological Series, Explanatory Notes, Sheet SE54-16. Australian Government Publishing Service, Canberra

Smith MA (1989) The case for a resident human population in the Central Australian ranges during full glacial aridity. Archaeol Ocean 24:93–105

Smith MA (1993) Biogeography, human ecology and prehistory in the sandridge deserts. Aust Archaeol 37:35–50

Smith MA (2009) Late Quaternary landscapes in Central Australia: sedimentary history and palaeoecology of Puritjarra rock shelter. J Quat Sci 24(7):747–760

Stahlschmidt MC, Miller CE, Ligouis B, Hambach U, Goldberg P, Berna F, Conard NJ (2015) On the evidence for human use and control of fire at Schöningen. J Hum Evol. doi:10.1016/j.jhevol.2015.04.004

Stein JK, Farrand WR (2001) Sediments in archaeological context. University of Utah Press, Salt Lake City

Stoops G (2003) Guidelines for analysis and description of soil and regolith thin-sections. Soil Science Society of America, Inc, Madison

Straus LG (1990) Underground archaeology: perspectives on caves and rockshelters. Archaeol Method Theory 2:255–304

Sullivan ME, Hughes PJ (1983) The geoarchaeology of the Sydney Basin sandstones. In: Young RW, Nanson GC (eds) Aspects of Australian sandstone landscapes, Australian and New Zealand Geomorphology Group Special Publication. University of Wollongong, Wollongong, pp 120–126

Thompson R, Oldfield F (1986) Environmental magnetism. Allen and Unwin, London

Tsatskin A, Nadel D (2003) Formation processes at the Ohalo II submerged prehistoric campsite, Israel, inferred from soil micromorphology and magnetic susceptibility studies. Geoarchaeology 18(4):409–432

Tsatskin A, Zaidner Y (2014) Geoarchaeological context of the later phases of Mousterian occupation (80–115 ka) at Nesher Ramla, Israel: soil erosion, deposition and pedogenic processes. Quat Int 331:103–114

Van der Marel HW, Beutelspacher H (1976) Atlas of Infrared Spectroscopy of Clay Minerals and their Admixtures. Elsevier Publishing Company, New York

Vannieuwenhuyse D, O'Connor S, Balme J (2016) Settling in Sahul: investigating environmental and human history interactions through micromorphological analyses in tropical semi-arid north-west Australia. J Archaeol Sci. doi:10.1016/j.jas.2016.01.017

Veth P (1989) Islands in the interior: a model for the colonization of Australia's arid zone. Archaeol Ocean 24:81–92

Veth P, Smith M, Bowler J, Fitzsimmons K, Williams A, Hiscock P (2009) Excavations at Parnkupirti, Lake Gregory, Great Sandy Desert: OSL ages for occupation before the Last Glacial Maximum. Aust Archaeol 69:1–10

Wallis LA, Keys B, Moffat I, Fallon S (2009) Gledswood Shelter 1: initial radiocarbon dates from a Pleistocene aged rockshelter site in northwest Queensland. Aust Archaeol 69:71–74

Wallis LA, Lowe KM, Popelka-Filcoff R, Bennett JW, St George C, Watson C, Fitzsimmons K, Lenehan C, Watchman A, Wight C, Matthews J (2014) Ochre through the late Quaternary at Gledswood Shelter 1, northwest Queensland. Unpublished paper presented at the Australasian Quaternary Association Biennial Conference, Mildura

Ward I (2004) Comparative records of occupation in the Keep River region of the eastern Kimberley, northwestern Australia. Aust Archaeol 59:1–9

Ward IAK, Larcombe P (2003) A process-orientated approach to archaeological site formation: application to semi-arid northern Australia. J Archaeol Sci 30:1223–1236

Williams AN, Veth P, Steffen W, Ulm S, Turney CSM, Reeves JM, Phipps SJ, Smith M (2015) A continental narrative: human settlement patterns and Australian climate change over the last 35,000 years. Quat Sci Rev 123:91–112

Woodward JC, Bailey GN (2000) Sediment sources and terminal Pleistocene geomorphological processes recorded in rockshelter sequences in northwest Greece. In: Foster IDL (ed) Tracers in geomorphology. Wiley, Chichester, pp 521–551

Woodward JC, Goldberg P (2001) The sedimentary records in Mediterranean rockshelters and caves: archives of environmental change. Geoarchaeology 16:327–354

Woodward JC, Hamlin RHB, Macklin MG, Karkanas P, Kotjabopoulou E (2001) Quantitative sourcing of slackwater deposits at Boila rockshelter: a record of late glacial flooding and Paleolithic settlement in the Pindus Mountains, Northwest Greece. Geoarchaeology 16:501–536